Measuring the Higgs sector

Rémi Lafaye,[a] **Tilman Plehn,**[b] **Michael Rauch,**[c] **Dirk Zerwas**[d] **and Michael Dührssen**[e]

[a] *LAPP, Université Savoie, IN2P3/CNRS,*
Annecy, France

[b] *Institut für Theoretische Physik, Universität Heidelberg,*
Heidelberg, Germany

[c] *Institut für Theoretische Physik, Universität Karlsruhe,*
Karlsruhe, Germany

[d] *LAL, IN2P3/CNRS,*
Orsay, France

[e] *Physikalisches Institut, Universität Freiburg,*
Freiburg, Germany

E-mail: Remi.Lafaye@lapp.in2p3.fr, Tilman.Plehn@cern.ch,
rauch@particle.uni-karlsruhe.de, zerwas@lal.in2p3.fr,
Michael.Duehrssen@cern.ch

ABSTRACT: If we find a light Higgs boson at the LHC, there should be many observable channels which we can exploit to measure the relevant parameters in the Higgs sector. We use the SFitter framework to map these measurements on the parameter space of a general weak-scale effective theory with a light Higgs state of mass 120 GeV. Our analysis benefits from the parameter determination tools and the error treatment used in new-physics searches, to study individual parameters and their error bars as well as parameter correlations.

Contents

1   Higgs physics at the LHC

Over the coming years, the main goal of LHC physics is to understand the breaking of the electroweak gauge symmetry. This symmetry we usually assume to be spontaneously broken, i.e. hidden by the presence of a non-symmetric vacuum. Such a vacuum can be induced through a gauge invariant Higgs potential involving powers of $H^\dagger H$, where H is a SU(2) Higgs doublet [1, 2]. One of the degrees of freedom of this doublet becomes a physical Higgs scalar, while the other three are absorbed as longitudinal degrees of freedom

into the massive W, Z gauge bosons. In this model all particle masses are proportional to the vacuum expectation value $v = 246\,\text{GeV}$, and the Higgs couplings to other particles as well as the Higgs itself are proportional to that particle's mass.

Gauge boson masses $m_{W,Z}$ arise from dimension-four $WWHH$ and $ZZHH$ terms. As the pseudo-Goldstone modes of the Higgs doublet are parts of the W, Z fields there is no additional free parameter in this construction. Both masses $m_{W,Z}$ are given by v times the gauge couplings g times a rotation by the electroweak mixing angle. This relation between the (measured) gauge boson masses and v allows us to determine v without observing the Higgs scalar.

Fermion masses arise from the dimension-four operators $H\Psi\overline{\Psi}$. This operator can be accompanied by any real dimensionless number, the Yukawa coupling y_f. Once the Higgs field develops a vacuum expectation value the combination $y_f \times v$ becomes the fermion mass. Note that in contrast to the gauge sector we have not yet measured any Higgs couplings to fermions, with the possible exception of y_t in the electroweak precision analysis [3, 4]. The link between the known fermion masses and the largely unknown Yukawa couplings can be offset for example by non-standard Higgs sectors.

A crucial question at the LHC will be: if we observe a light scalar particle, how can we tell that this state is the physical Higgs boson and not something else or a mixture between a Higgs boson and another new state. A good example for a state which looks like a Higgs scalar and mixes with a Higgs scalar is the radion in theories with large warped extra dimensions [5]. A more conservative modification of the Higgs sector in the Standard Model could be an extension, for example by another Higgs doublet. A theory which requires such an extended Higgs sector is supersymmetry, where we find two CP-even scalar Higgs bosons which mix, leading to a light and a heavy mass eigenstate [6, 7]. In the decoupling limit the lighter of these mass eigenstates becomes the Standard Model Higgs boson, but for finite supersymmetric and heavy-Higgs mass scales its properties deviate from the Standard Model case.

Our strategy for studying the Higgs sector is analogous to our studies of new-physics parameter spaces [8]: there are many pieces of information on the Higgs sector which are not continuous. These include the spin of the Higgs boson, its CP quantum numbers, or the structure of a CP-even WWH vertex [9]. In this paper we study the continuous Higgs parameters, i.e. we assume that these quantum numbers are known, or in other words, we assume that we know the operator basis we need to include in the effective Lagrangian describing Higgs physics at the LHC. However, for each of these operators we have to determine its strength, to then compare the result with the Standard Model or alternative weak-scale theories.

Such an analysis will test all accessible Higgs couplings to known particles for a given Higgs mass [10–12], which we assume to be $120\,\text{GeV}$. This will first of all include the gauge boson couplings, where as mentioned above we have little room to alter the relations of the gauge boson masses and the gauge couplings. In addition, we will measure the Yukawa couplings and compare them to the known fermion masses. The observable Higgs channels at the LHC involve gluon fusion as well as weak boson fusion combined with a large number of branching ratios. Such an analysis will be statistically challenging. Just as the high-

dimensional parameter space analyses studying new physics in the LHC era, the analysis needs to focus on the proper treatment of all errors [8, 13].

Some Higgs couplings will most likely only be measured at a later stage, involving integrated luminosities of at least 300 fb^{-1}. One of them is the only second-generation Higgs decay we might observe at the LHC, the decay into muons [14, 15]. Owed to the outstanding $m_{\mu\mu}$ resolution in particular of CMS the weak-boson-fusion channel might come close to a 5σ signal using modern analysis tools. However, because of the lack of experimental studies and due to this small event rate we neglect all light-flavor Yukawa couplings in this analysis.

Extracting the one-loop Higgs coupling to $Z\gamma$ is similar to the two-photon channel in suffering from a reduced branching ratio, plus an additional leptonic branching ratio of the Z boson. We do not include it in our analysis, because of its small event rate for low-luminosity running.

Involving physics beyond the Standard Model a light Higgs can decay to invisible particles. The issue in searching for this decay is triggering the events, which should be possible for weak boson fusion production [16]. Then, we can extract an invisible Higgs signal from an invisible Z decay using kinematic distributions and a careful analysis of signal-free control regions. Note that because of the limited energy it is unlikely that such a signal would be mimicked by the production of for example two neutralinos or charginos, because phase space essentially only allows for the production of one particle in this channel at the LHC [17].

Last but not least, the arguably hardest-to-measure Higgs coupling can be regarded as the most interesting: if the electroweak symmetry is really spontaneously broken, this means there exists a Higgs potential. Such a potential can only exist if there is a Higgs self coupling. While the $W_L W_L H$ coupling is induced by such a self coupling, it would be most desirable if we could measure the explicit self coupling λ_{HHH} at the LHC [18]. Finally, a measurement of the quartic self coupling λ_{HHHH} could confirm the actual form of the Higgs potential [19], but it is unlikely that we will measure this last and final Higgs parameter at any collider currently discussed, including the VLHC or CLIC [20]. We skip such high-luminosity channels which should not feed back into our leading parameter set. The analysis presented in this paper can easily be extended.

The final assumption we make for the structure of the Higgs sector is CP symmetry. While in many new-physics models, like supersymmetry, it is actually hard to avoid additional CP violation we currently have no experimental hints for such complex phases in the weak-scale Lagrangian [21]. In other words, the apparent absence of additional CP violation from the TeV scale could be considered one of the worst problems of TeV-scale model building; it serves as a benefit for our Higgs parameter analysis.

Any parameter study at the LHC or elsewhere needs to focus on the error analysis. First of all, this means that we have to include statistical and systematic errors including a full correlation matrix as well as theory errors. The latter are numerically challenging, because they are not Gaussian. From these errors we need to construct a likelihood map over the entire parameter space, for example using Markov Chains or simulated annealing. The techniques we employ to scan the high-dimensional parameter space can have a large

impact on the numerical efficiency, but they should be equivalent in the final result. One major technical difference between these methods is the study of secondary maxima in the likelihood map.

An exclusive likelihood map is well suited for example to study correlations between different model parameters, i.e. different Higgs couplings, as well as local properties of the likelihood map. However, there are good reasons to ask more specific questions. The most obvious are about the probability or likelihood distribution of one Higgs coupling (e.g. g_{WWH}) or the correlation of two of them (e.g. g_{WWH} vs $g_{\tau\tau H}$). The answer to this question depends on how we ask this questions, and what methodology we want to employ.

Bayesian probability distributions and frequentist profile likelihoods are two ways to study a parameter space, where some model parameters might be very well determined, others heavily correlated, and even others basically unconstrained. Both of them rely on an exclusive likelihood map as a starting point. Following the SFitter strategy we carefully compare the benefits and disadvantages of the frequentist and the Bayesian approaches for each model parameter.

The approach of mapping measurements onto a high-dimensional parameter space for example realized in SFitter [8] (or in the largely similar Fittino tool [13]) are completely general: model parameters as well as measurements are included in the form of model and measurement files and can simply be replaced. SFitter serves as a general tool to map typically up to 20-dimensional highly complex parameter spaces onto a large sample of highly correlated measurements of different quality including a proper error treatment. While this approach is obviously mandatory for high-precision analyses, it is also best suited to extract the maximum information from any kind of correlated measurements.

2 LHC measurements

2.1 Production modes

At the LHC we rely on two main production processes for a Standard-Model type Higgs boson: through a top loop the Higgs couples to two gluons, which leads to cross sections of the order of $10 - 100$ pb (37 pb for a 120 GeV Higgs). The production cross section is known at next-to-leading order including all top-mass effects [22, 23]. At NNLO the gluon-fusion production rate is known for an effective ggH coupling [24], where the description of gluon radiation off the top loop might not reproduce all distributions correctly. Due to unknown higher orders we assume a theory uncertainty of 13% on the production rate after acceptance and background rejection cuts [25]. This error includes the uncertainty on a jet veto for $H \to WW$ decays [26]. For a realistic analysis including actual LHC data we would have to check in detail that cuts or analysis strategies do not lead to large additional errors, for example by inducing large logarithms [27, 28].

The second largest production cross section is mediated by weak boson fusion, involving two forward jets with transverse momentum around $m_W/2$ and typical cross sections of $1 - 10$ pb (4.5 pb for a 120 GeV Higgs). From a QCD perspective this production channel is particularly clean, because there is no color flow between the two DIS sides of the process. This simple fact we can make use of by vetoing central jets between the two forward tagging

jets [29]. The total rate as well as the key distributions for this signal are known to next-to-leading order [30], including (as it turns out: negligible) interference effects [31]. An interesting aspect is that due to the suppression of higher-order QCD effects, strong and electroweak NLO corrections are of the same size but opposite sign. For this production process we estimate the theory error to range around 7% [30].

For weak boson fusion there remains a caveat: Higgs rate measurements include the survival probability of a central minijet veto [29]. It is one of the reasons why weak boson fusion signatures have such a spectacular signal-over-background ratio. While we will be able to measure this veto probability in Z+jets production [32] for the signal we need to predict it [33] — including the underlying event. While surely a minijet veto will work in LHC analyses, in section 5.4 we will check what happens to the Higgs sector analysis with an increased error.

The production channels of gluon fusion and weak boson fusion are not independent. Higgs boson production with two jets will have contributions from both gluon fusion and weak boson fusion. With appropriate cuts, we can enhance one channel over the other [34], but in our rate analysis we nevertheless need to include both. We do not introduce an additional error for this separation, assuming it to be already covered by the theory errors and the systematic errors.

A third production mechanism is the radiation of a Higgs boson off top pairs. This signature, in spite of its sizable rate of up to 600 fb (450 fb for a 120 GeV Higgs), suffers from its high-multiplicity final state and hence large combinatorial errors. Essentially, any Higgs decay product will also be present in the top decays. Its rate is known to next-to-leading order [35], with a remaining theory error around 13%.

Last, but not least, there might be hope to see a Higgs boson produced in association with a W or Z gauge boson. Its reasonable rate of $0.3 - 3$ pb (2.2 pb for a 120 GeV Higgs) suffers from the additional leptonic branching ratio of the gauge bosons. Still, in particular in the context of modern jet-structure driven searches this production channel could well turn out useful if we combine it with a Higgs decay with a large branching ratio. For this channel we assume a theory error of 7%.

Throughout this analysis we will skip the analysis of Higgs pair production [36]. In the Standard Model this channel has a one-to-one correlation with the Higgs self coupling [18] and is strongly suppressed. We note, however, that in models with additional Higgs resonances the pair production of light Higgs bosons might well be visible [37].

2.2 Signatures

The challenge for Higgs searches at the LHC lies in triggering and the extraction of the signal from backgrounds. In our analysis we use the following list of most promising signatures for models not too different from the Standard Model [38]. This list should not be considered the final work for the LHC, but simply reflects our understanding at the current stage of Monte-Carlo studies:

- $H \rightarrow b\bar{b}$ — while for small Higgs masses this is the dominant decay channel, with branching ratios up to 90%, it is particularly hard to extract from QCD backgrounds.

Recent CMS and Atlas studies show that combinatorial backgrounds make it very hard to observe this decay in $t\bar{t}H$ production, where it might never reach the 5σ level [39]. The best chance for this decay channel will probably be the WH/ZH production mode [40] with a subjet analysis [41], currently under study by both collaborations.

- $H \to WW$ — even though two leptonic W decays only allow us to reconstruct a transverse mass of the WW pair this channel is arguably the most powerful search channel for a light Higgs boson. In the gluon fusion process, where the most important observables to cut on are correlations between the two leptons this decay signature can be extracted using the opening angle of the two leptons (being small if the two W bosons come from a resonant scalar) [26]. In weak boson fusion, this decay can be used even if one of the Ws is far off-shell [42] with a spectacular $S/B \sim \mathcal{O}(1)$. Combined with the $t\bar{t}H$ production mode this decay might turn out useful for on-shell decays [43], so we include all three production mechanisms.

- $H \to ZZ$ — due to its spectacular fully reconstructable four-lepton final state this signature is usually referred to as the 'golden channel'. It works in combination with the gluon fusion [44] as well as with the weak boson fusion [45] production process, but is somewhat statistically limited to larger Higgs masses.

- $H \to \tau\tau$ — for this channel to be useful we need to reconstruct the invariant mass of the two taus. It is well known how to do this in the collinear approximation, where the taus are fast-moving [46]. Unfortunately, because of the steep gluon densities, gluon fusion produces Higgs bosons too close to threshold, which means we cannot use this production mechanism. In contrast, in weak boson fusion the Higgs recoils against the two tagging jets, so the taus are boosted. That way we can even measure the Higgs mass to $\sim 5\,\mathrm{GeV}$ [47]. Further improvement we expect from an improved statistical distinction of the signal from the $Z \to \tau\tau$ background [48]. For the $t\bar{t}H$ production channel with a subsequent decay to taus we are not aware of experimental studies, so we leave it out for now [49].

- $H \to \gamma\gamma$ — the decay to two photons has the advantage of being the only fully reconstructable channel for a very light Higgs boson, as preferred by electroweak precision data. The $\gamma\gamma$ mass resolution of $2\,\mathrm{GeV}$ or better compensates for the small branching ratio and makes this decay channel a promising candidate for an observation in gluon fusion production [50], weak boson fusion production [51] and even $t\bar{t}H$ associated production [52]. Moreover, this channels allows us to measure the mass of a light Higgs boson with a precision $\mathcal{O}(100\,\mathrm{MeV})$, depending on the Higgs mass.

- $H \to$ invisible — the best chance to observe a Higgs decay to invisible particles [53] is in combination with weak boson fusion, namely looking for two tagging jets recoiling against missing energy [16]. Of course, the determination of the Higgs branching ratio to invisible new states relies on our understanding of the production rate and

therefore on the proper combination with all other Higgs signatures. Due to the lack of a full-simulation analysis, we do not include this signal as a measurement. On the other hand, because this decay channel can be of crucial importance for new-physics searches, we include it as an additional free parameter in part of our analysis.

Because of the recent developments in the $H \rightarrow b\bar{b}$ channels we briefly mention other strategies to see this Higgs decay at the LHC: first, there might be a faint chance to observe the $b\bar{b}$ decay directly in weak boson fusion. Producing a single Higgs boson might lead to a $2.9 - 5.2\sigma$ signal with 600 fb^{-1} of triggered data [54]. Secondly, we can look for a Higgs boson produced in association with a W boson in weak boson fusion. This signature has been estimated to lead to a 4.4σ signal with 200 fb^{-1} of data including a functioning central jet veto [55]. The channel has been reanalysed recently leading to a significance $S/\sqrt{B}$ of about 1.8 [56] for 100 fb^{-1}. Both of these analyses we do not include due to their limited potential during low luminosity running and a lack of full simulation. Last but not least, we can look for a hard photon and a Higgs in weak boson fusion [57]. For this channel we might expect a 1.2σ significance for an integrated luminosity of 30 fb^{-1} with a signal-to-background ratio around 1/20. The inclusion of a mini-jet veto, studied qualitatively in ref. [57], would lead to an improvement by a factor 2 [57]. When discussing the $t\bar{t}H$ production channel with a Higgs decay to bottoms we should therefore keep in mind that its impact could be improved significantly after including $H\gamma$ production or similar channels in weak boson fusion.

Note that including signal and background contributions to counting experiments makes it obvious that the rate measurements discussed above only rarely fulfill the ideal condition $S \gg B$. Instead, for gluon-fusion signatures we find that the number of signal events tends to be significantly smaller than the number of background events, with the positive aspect that for example in the $H \rightarrow \gamma\gamma$ channel a side bin analysis allows us to very precisely subtract the background events. For weak boson fusion signatures the ratio S/B typically looks better, but on the down side the event numbers are comparably small, which in some channels forces us into the Poisson region.

In our numerical analysis we use predictions for the production rates as described in ref. [58]. These we table the points and interpolate between them. For the branching ratios we use Hdecay [59], modified to allow for arbitrary Higgs coupling values. To estimate the effect of cuts, we compute an efficiency factor from our rates and the values given in ref. [60]. Compared to this study we reduce the signal rate for $t\bar{t}H, H \rightarrow b\bar{b}$ by 50%, in agreement with recent Atlas [39, 61] and CMS [62] studies. For the $WH/ZH, H \rightarrow b\bar{b}$ channel including a subjet analysis we use the rates given in the original paper [41] and check for an effect of a degradation through detector effects in section 5.3.

2.3 Errors

In order to obtain reliable error estimates for the Higgs sector parameters, a proper treatment of experimental and theory errors depending on their origin is mandatory. We follow the CKMfitter prescription or Rfit scheme [63]. The complete set of errors includes statistical experimental errors, systematic experimental errors, and theory errors. The statistical

production	decay	$S + B$	B	S	$\Delta S^{(\text{exp})}$	$\Delta S^{(\text{theo})}$
$gg \to H$	ZZ	13.4	6.6 ($\times$ 5)	6.8	3.9	0.8
qqH	ZZ	1.0	0.2 ($\times$ 5)	0.8	1.0	0.1
$gg \to H$	WW	1019.5	882.8 ($\times$ 1)	136.7	63.4	18.2
qqH	WW	59.4	37.5 ($\times$ 1)	21.9	10.2	1.7
$t\bar{t}H$	$WW(3\ell)$	23.9	21.2 ($\times$ 1)	2.7	6.8	0.4
$t\bar{t}H$	$WW(2\ell)$	24.0	19.6 ($\times$ 1)	4.4	6.7	0.6
inclusive	$\gamma\gamma$	12205.0	11820.0 ($\times$ 10)	385.0	164.9	44.5
qqH	$\gamma\gamma$	38.7	26.7 ($\times$ 10)	12.0	6.5	0.9
$t\bar{t}H$	$\gamma\gamma$	2.1	0.4 ($\times$ 10)	1.7	1.5	0.2
WH	$\gamma\gamma$	2.4	0.4 ($\times$ 10)	2.0	1.6	0.1
ZH	$\gamma\gamma$	1.1	0.7 ($\times$ 10)	0.4	1.1	0.1
qqH	$\tau\tau(2\ell)$	26.3	10.2 ($\times$ 2)	16.1	5.8	1.2
qqH	$\tau\tau(1\ell)$	29.6	11.6 ($\times$ 2)	18.0	6.6	1.3
$t\bar{t}H$	$b\bar{b}$	244.5	219.0 ($\times$ 1)	25.5	31.2	3.6
WH/ZH	$b\bar{b}$	228.6	180.0 ($\times$ 1)	48.6	20.7	4.0

Table 1. Signatures included in our analysis for a Higgs mass of $120\,\text{GeV}$. The Standard Model event numbers for 30 fb^{-1} include cuts [60]. The factor after the background rates describes how many events are used to extrapolate into the signal region. The last two columns give the one-sigma experimental and theory error bars on the signal.

luminosity measurement	5 %
detector efficiency	2 %
lepton reconstruction efficiency	2 %
photon reconstruction efficiency	2 %
WBF tag-jets / jet-veto efficiency	5 %
b-tagging efficiency	3 %
τ-tagging efficiency (hadronic decay)	3 %
lepton isolation efficiency ($H \to 4\ell$)	3 %

	$\Delta B^{(\text{syst})}$	corr.
$H \to ZZ$	1%	yes
$H \to WW$	5%	no
$H \to \gamma\gamma$	0.1%	yes
$H \to \tau\tau$	5%	yes
$H \to b\bar{b}$	10%	no

Table 2. Systematic errors used in our analysis. Left: systematic errors applying to both signal and background. Reconstruction and tagging efficiencies are defined per particle, e.g. $H \to \gamma\gamma$ has a 4% error on the photon reconstruction. Right: systematic background errors, either fully correlated or independent between channels. Tables same as ref. [60].

experimental errors are treated as uncorrelated in the measured observables. In contrast, the systematic experimental errors for example from the luminosity or from tagging efficiencies are fully correlated.

As efficiency factors are usually determined from other observed channels, they really behave like statistical errors and should therefore be Gaussian. The numerical values for systematic errors we take from ref. [60]. For convenience, we have included them in table 2.

In contrast, theory errors reflecting unknown higher orders in perturbation theory should not be Gaussian but flat box-shaped within a certain range of validity of perturbation theory. In other words, the probability assigned to any measurement does not depend on its actual value, as long as it is within the interval covered by the theory error. There could be a tail attached to these theory-error distributions, but higher-order corrections

σ (gluon fusion)	13 %
σ (weak boson fusion)	7 %
σ (VH-associated)	7 %
σ ($t\bar{t}$-associated)	13 %

BR($H \to ZZ$)	1 %
BR($H \to WW$)	1 %
BR($H \to \tau\bar{\tau}$)	1 %
BR($H \to c\bar{c}$)	4 %
BR($H \to b\bar{b}$)	4 %
BR($H \to \gamma\gamma$)	1 %
BR($H \to Z\gamma$)	1 %
BR($H \to gg$)	2 %

Table 3. Theory errors used in our analysis for a 120 GeV Higgs.

are definitely not allowed to become arbitrarily large. Confronted with a perturbatively unstable observable one would instead have to rethink the perturbative description of the underlying theory. The numerical size of the theory errors we give in table 3. The branching ratios to $c\bar{c}$ and gg do not enter in any measurements but indirectly via the total width of the Higgs boson. To be consistent with our approach of flat theory errors the propagation of errors is linear and not quadratic.

The error due to a mini-jet veto survival probability in background processes behaves like any other efficiency, i.e. Atlas and CMS measure it in signal-free phase space regions and assign a Gaussian error. However, for the signal rate we have to rely on theory to predict the survival probability. Hence, it is a fully correlated flat error which we can add to the error on the production cross section in weak boson fusion.

Defining a scheme for flat theory errors includes their combination with the (Gaussian) experimental errors. A simple (Bayesian) convolution leads to the difference of two one-sided error functions with a clear maximum, so the convolution knows about the central value of theory prediction. A better solution is a distribution which is flat as long as the measured value is within the theoretically acceptable interval and then drops off like a Gaussian with the width of the experimental error, the Rfit profile likelihood construction [63]. The log-likelihood $\chi^2 = -2\log\mathcal{L}$ given a set of measurements $\vec{d}$ and in the presence of a general correlation matrix then C reads

$$\chi^2 = \vec{\chi}_d^T \, C^{-1} \, \vec{\chi}_d$$

$$\chi_{d,i} = \begin{cases} 0 & |d_i - \bar{d}_i| < \sigma_i^{(\text{theo})} \\ \dfrac{d_i - \bar{d}_i + \sigma_i^{(\text{theo})}}{\sigma_i^{(\text{exp})}} & d_i - \bar{d}_i \, < -\sigma_i^{(\text{theo})} \\ \dfrac{d_i - \bar{d}_i - \sigma_i^{(\text{theo})}}{\sigma_i^{(\text{exp})}} & d_i - \bar{d}_i \, > \sigma_i^{(\text{theo})} \, , \end{cases} \qquad (2.1)$$

where $\bar{d}_i$ is the i-th data point predicted by the model parameters and d_i the actual measurement. Flat errors lead to a technical complication with hill-climbing algorithms. Functions describing box-shaped error distribution will have a discontinuities of higher derivatives. The Rfit scheme has a step in the second derivative which we need to accommodate. As a second complication the log-likelihood becomes constant in the central region, so some parameters vanish from the counting of degrees of freedom [8]. If all experimental errors

are Gaussian, $\sigma^{(\mathrm{exp})}$ of eq. (2.1) is the convolution of the errors, i.e. the square-root of the sum of the squares of the experimental errors. The off-diagonal elements of the correlation matrix C are constructed by a generalization of eq. (2) of [8].

The uncertainty on the mass of top and bottom quarks is another source of errors which we need to take into account. For these measurements we use a single experimental error each which comprises all different sources and is uncorrelated to any other measurement. Its numerical size is 1.0 and 0.07 GeV for top and bottom quarks, respectively.

For the experimental errors the systematic parts are inferred from large data samples, and it is safe to assume them as Gaussian. On the other hand, in some of the Higgs channels we will only observe a few events, so we need to use a Poisson distribution to model the behavior correctly. Therefore, we use Poisson statistics for all statistical errors. Our method of combining Gaussian and Poisson errors affecting the same measurement we describe in detail in appendix A. Unless explicitly stated otherwise, SFitter uses smeared toy measurements to evaluate the errors. For each toy measurement we determine the best-fit value, which means the width of the distribution of the best-fit values gives the error on the model parameters.

3 General Higgs sector

As sketched earlier, we allow for a general Higgs sector including couplings to all Standard-Model particles and an invisible final state. We assume that we observe a narrow 120 GeV Higgs candidate as a peak either in the $\gamma\gamma$ or ZZ invariant masses, in the collinearly reconstructed invariant $\tau\tau$ mass, or in the transverse mass of WW pairs. This most notably means that we are searching for two-particle decays of the Higgs boson, which has an important consequence: if the Higgs boson were to couple strongly to light-flavor jets (which are swamped by QCD backgrounds) this would reduce the fraction of Higgs bosons decaying into visible channels, but it would also enhance the production cross section at the LHC. We discuss such a scenario as well as invisible Higgs decays in section 4.3. As mentioned in the introduction, we will not take into account Higgs couplings which might be visible in high-luminosity running in a single channel and/or are not expected to feed back into the determination of the leading Higgs parameters. This includes the Higgs-muon Yukawa coupling, the Higgs self coupling, or invisible Higgs decays. Such channels can be very useful to further understand the Higgs sector, but their results can be considered purely additional to our analysis.

For the tree-level Standard Model Higgs couplings to any particle j we allow for a deviation

$$g_{jjH} \longrightarrow g_{jjH}^{\mathrm{SM}} \ (1 + \Delta_{jjH}) \tag{3.1}$$

where the Δ_{jjH} are independent of each other. If necessary redefining our Higgs field we can without loss of generality assume that one of the tree-level Higgs couplings is positive, i.e. $g_{WWH} > 0$ or $\Delta_{WWH} > -1$. Note that these couplings are of mass dimension three for gauge bosons and four for fermions, so they are part of the renormalizable Lagrangian. In the minimal one-doublet Higgs sector such corrections spoil gauge invariance. This can

be cured for example by additional heavy Higgs states which we integrate out to define an effective one-Higgs-doublet Standard Model with free couplings.

In addition, there are three relevant loop induced couplings in the Higgs sector: $g_{ggH}, g_{\gamma\gamma H}$ and $g_{\gamma ZH}$. Such couplings are sensitive to new particles in the spectrum, like for example supersymmetry or a chiral fourth generation. In the latter case the Tevatron limits on $gg \to H \to WW$ strongly constrain the allowed Higgs masses in the presence of such a heavy generation which leads to an enhancement of the production rate roughly by a factor 9 [64]. Including a general new-physics scale Λ [19, 66] such couplings arise in the effective Lagrangian as

$$\mathcal{L} \supset \frac{g_{ggH}}{\Lambda} (G^a)^{\mu\nu}(G^a)_{\mu\nu} + \frac{g_{\gamma\gamma H}}{\Lambda} F^{\mu\nu} F_{\mu\nu} \tag{3.2}$$

Note that in general new-physics models these couplings do not have to be perturbatively suppressed, as they are in the Standard Model or in the MSSM. In our weak-scale analysis we consider two different sources of higher-dimensional couplings: first, there are known Standard Model particles propagating in loops and inducing them, so any change in the tree-level couplings eq. (3.1) propagates into the one-loop effective couplings. Secondly, we allow for manifestly dimension-five operators from new physics

$$g_{jjH} \longrightarrow g_{jjH}^{\mathrm{SM}} \left(1 + \Delta_{jjH}^{\mathrm{SM}} + \Delta_{jjH}\right) \tag{3.3}$$

where g_{jjH}^{SM} is the loop-induced coupling in the Standard Model, $\Delta_{jjH}^{\mathrm{SM}}$ is the contribution from modified tree-level couplings to Standard-Model particles, and Δ_{jjH} is an additional dimension-five contribution, for example from new heavy states.

The ansatz described above describes our general effective theory of the Higgs sector, allowing for deviation from the Standard Model values. Such deviations will be loop induced even in the Standard Model. If we allow for new physics in electroweak symmetry breaking such loop effects can be enhanced by large loop corrections, a strongly interacting sector mimicking a scalar Higgs boson, or an extended Higgs sector. We can illustrate this using g_{WWH}: if we were to measure a smaller value than the Standard Model prediction this could point to additional Higgs fields sharing the burden of creating the correct gauge boson masses $v^2 = v_1^2 + v_2^2 + \cdots$ This kind of behavior we know from the type-II two-Higgs-doublet model of the MSSM where the couplings of the two Higgs scalars to the weak gauge bosons are split according to $\sin^2(\beta - \alpha) + \cos^2(\beta - \alpha) = 1$.

A too large value of g_{WWH}, in contrast, could point towards the existence of an additional higher-dimensional operator. The way to check such a hypothesis would involve an analysis of angular correlations which can distinguish different tensor structures of the WWH coupling in weak boson fusion, independent of the decay channel [9].

One basic assumption we have to make for the Higgs sector analysis is the treatment of the total width, which can be varied just like the couplings

$$\Gamma_{\mathrm{tot}} = \Gamma_{\mathrm{tot}}^{\mathrm{SM}} (1 + \Delta_\Gamma) \quad . \tag{3.4}$$

Allowing for a simultaneous scaling of all couplings and the total width we see that as long as we keep $g^4/\Gamma_{\mathrm{tot}} = C$ finite and constant, none of our ($\sigma \cdot$ BR) measurements will be

affected and the shift in the couplings will not be observable. Keeping this ratio and hence all measurements unaffected implies that for example a theory-motivated upper limit on any of the relevant couplings translates into an upper limit on the total Higgs width, and vice versa.

Limiting ourselves to Higgs singlets and doublets we can derive such an upper limit on g_{WWH} from the perturbative unitarization of $WW \to WW$ scattering. As seen in the last paragraph, the unitarization of this process can be shared by several Higgs states, but since their couplings to gauge bosons enter twice per amplitude it leads to strictly a sum of the individual contributions. In other words, no individual WWH_j coupling of any of the Higgs states j contributing can be larger than the value which alone unitarizes this process, i.e. g_{WWH}^{SM}. This upper limit on g_{WWH} can be translated into an upper limit on the total width. As mentioned in the last paragraph, this argument is limited to dimension-three WWH operators and for example breaks down in the limit of strong dimension-five interactions as shown in eq. (3.3).

In a similar manner, we can obtain a lower limit on the Higgs width: obviously, the total width is at least as large as the sum of all observable partial widths. However, these partial widths are computed from the extracted couplings, and the couplings can be dialed to zero as long as the total width vanishes simultaneously. We can insert the scaling behavior $\Gamma_{\text{vis}} \propto g^2$ into the expression for C, add an additional positive contribution $\Gamma_x(g) > 0$ with an arbitrary g dependence and compute the small-coupling limit

$$C = \lim_{g^2 \to 0} \frac{g^4}{\Gamma_{\text{tot}}} = \lim_{g^2 \to 0} \frac{g^4}{g^2(\Gamma_{\text{vis}}/g^2) + \Gamma_x} = 0 \quad . \tag{3.5}$$

However, by definition this ratio C has to be finite to protect our rate measurements, which means that we cannot actually dial down all partial widths simultaneously. Instead, we have to consider a quadratic equation in g^2 which indeed returns a lower limit on the couplings and hence the total width. It is obvious for any such argument that the knowledge of as many as possible partial widths and therefore the observation of $H \to b\bar{b}$ decays is crucial for studies like this.

For a light Standard-Model Higgs boson, the difference between the observable partial width at the LHC and the Standard Model width is of the order of $\lesssim 10\%$. Identifying the total width with the sum of the observed partial widths is practically equivalent to including an upper limit. Therefore, throughout this analysis we always simply identify the total width with the sum of the observed partial widths. Unless explicitly mentioned this includes all Standard Model particles listed in section 2. An example scenario how this might mislead us we discuss in section 4.3.

4 Higgs likelihood map

Due to the number of possible observable channels for a light Higgs boson, the LHC should be able to not just discover a narrow scalar state which might or might not be the Standard-Model Higgs boson, but tell if such a state has anything to do with the Standard Model Higgs boson. This is a statistical statement, in which all errors and the resulting confidence

level for a given hypothesis play a crucial role. Therefore, it is vital to control the mapping of the high-dimensional space of correlated measurements onto the high-dimensional Higgs parameter space. Just like for any other parameter study, the starting point of such a study is a completely exclusive likelihood map.

Such a likelihood map is a large list or array of points in model space with their corresponding probability to agree with the given data. We can construct it using Markov chains where the points in the Markov chain represent the entire parameter space in their probability to agree with a data set. In principle, we could evaluate any kind of function on this Markov chain, similar to general mass scales or dark matter properties in analyses of physics beyond the Standard Model [67–69]. In this analysis we are only interested in the probability to agree with data itself which in the case of supersymmetric parameters led us to consider weighted Markov chains [8].

The problem with such an exclusive likelihood map is that it is (a) hard to graphically represent and (b) hard to interpret once we for example want to know if one individual coupling agrees with the Standard Model or does not. However, to reduce the dimensionality of the parameter space we have to decide on a scheme, namely Bayesian probabilities or profile likelihoods.

If we want to maintain the mathematical properties of a probability distribution and compare the height and size of different peaks we need to integrate over the unwanted directions, which means we need to define an integration measure in model space. Such a measure is always a free choice, a prior, and the resulting Bayesian probability distribution will depend on it. The model space integration also leads to volume effects, just like the usual example — is a water molecule more likely to be found in a highly concentrated spoon of water or in a huge cloud? Moreover, the integration will produce noise effects which can obscure narrow structures in the parameter space.

Alternatively, we can construct a likelihood without introducing any measure, for example by simply picking the best point in the unwanted direction and identify it with the value in the reduced likelihood map. The result is referred to as a profile likelihood, has no noise effects and is designed to best represent the structures of the original likelihood. However, it does not allow us to compare the integrated size of different peaks of alternative solutions in the parameter space.

In our new-physics parameter analyses [8] we have learned that we can extract the most information by showing both, a Bayesian probability as well as a profile likelihood, side by side, accepting that they do not have to give the same answers because they are not the same question. In this analysis we will find that correlations around a well-defined central fit value are more important than distinct equally good solutions, which implies that we will rely largely on profile likelihoods.

Due to the probability distribution function which chooses their next point Markov chains are intrinsically Bayesian. Correspondingly, we find that profile likelihoods are harder to extract. To improve this behavior we can cool down the Markov chains to improve the resolution of local structures, provided we ensure that we do not miss structures in parameter space. If we slowly dial down the random number which decides whether a worse point is still accepted, we start scanning the parameter space similar to a standard
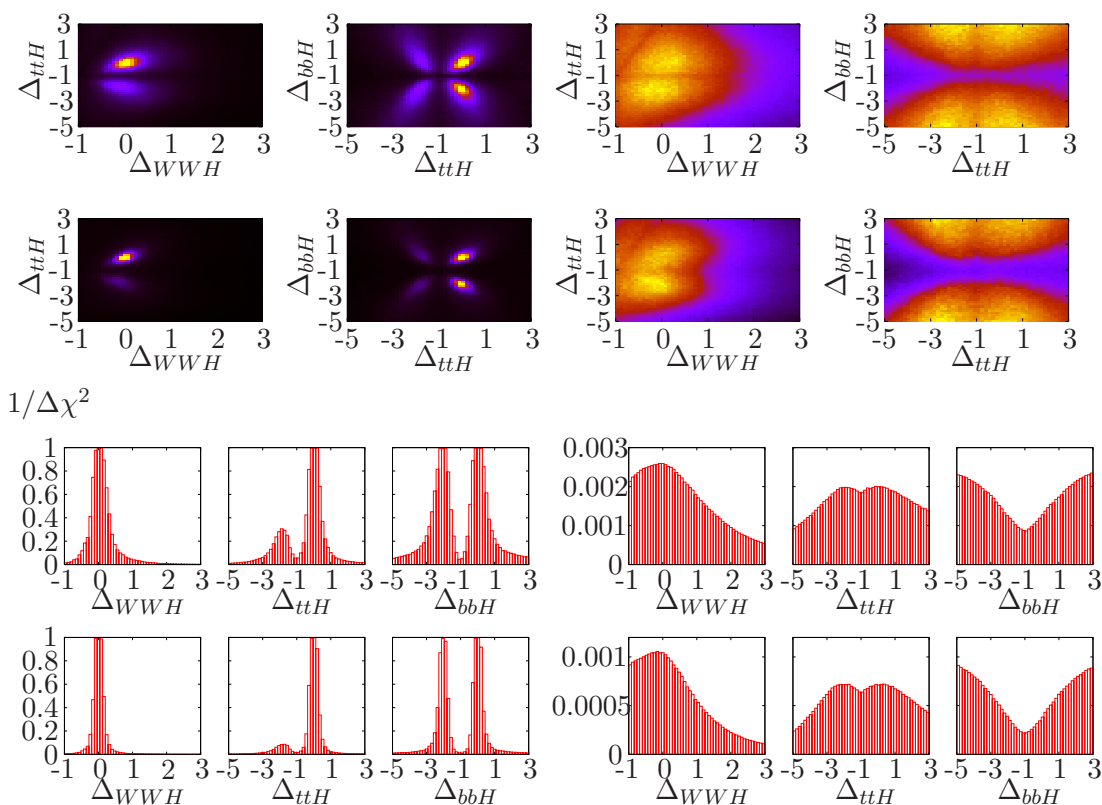
Figure 1. Profile likelihoods (left) and Bayesian probabilities (right) for the WWH, ttH, and bbH couplings. Not allowing for additional ggH or $\gamma\gamma H$ couplings we show results for 30 fb^{-1} and for 300 fb^{-1} in the upper and lower rows. The Higgs mass is chosen as 120 GeV. All experimental and theory errors are included. Here and in all other figures we assume the WWH coupling to be positive, i.e. $\Delta_{WWH} > -1$.

Markov chain and then slowly concentrate on one structure. This cooling significantly improves the resolution of local structures around a peak and thereby yields a much better resolution for profile likelihoods. More details of this approach we give in appendix B.

4.1 Parameters and correlations

Given the set of measurements described in section 2 it is obvious that most of the Standard Model couplings should be accessible to a full analysis. Nevertheless, we start with a minimal set of Higgs sector parameters in which we only allow for tree-level couplings to all Standard Model particles. This implies that there are no new particles contributing to the effective ggH and $\gamma\gamma H$ couplings. Since we compute the Higgs width as the sum of all visible partial widths, a measurement of the bottom Yukawa constitutes the main fraction of the Higgs width.

Based on the studies of weak boson fusion we limit our study to low-luminosity running and a conservative integrated luminosity of 30 fb^{-1}. We can easily test how constraining this assumption is for our analysis: without including any effective higher-dimensional

couplings we estimate the effect of an increase in luminosity from the standard 30 fb^{-1} to 300 fb^{-1}. Figure 1 shows that the existence of correlations is independent of the integrated luminosity, i.e. these correlations are physical, and even the relative weights of alternative solutions hardly depend on the luminosity. Note that just like the entire analysis the error on the Higgs rates does not decrease like $1/\sqrt{S}$ but that we always include backgrounds, which makes $S + B$ the relevant number of events.

Moving on, one striking feature in figure 1 is the alternative minimum for a negative top Yukawa coupling. In the comparison between profile likelihood and Bayesian probability we see that while the best-fit point clearly prefers the correct sign of the top Yukawa, volume effects wash out this distinction in the Bayesian probability. The only term which breaks this sign degeneracy is the loop-induced $g_{\gamma\gamma H}$, which only allows for a synchronized sign flip of g_{ttH} and g_{WWH}. The positive correlation between these two couplings shown in the two-dimensional panel of figure 1 arises on the one hand because of the strong destructive interference of the two loops and on the other hand due to a possible approximate scaling of all tree-level couplings compensating a shift in the less well measured bottom Yukawa coupling. A $g_{WWH} - g_{bbH}$ correlation shows the same kind of positive correlations for the same two reasons. As the g_{bbH} Yukawa coupling is small, a small shift in g_{WWH} or g_{ttH} compensates a major change in g_{bbH}. However, such a large shift in the bottom Yukawa coupling is not completely out of the world — in the supersymmetric two-Higgs-doublet model the additional parameter $\tan\beta$ plays exactly this role.

From the one-dimensional histograms in figure 1 we see that the LHC provides a very reasonable measurement of the top Yukawa coupling via the effective ggH coupling. The bottom Yukawa coupling is better constrained than in previous analyses using the $t\bar{t}H$ production channel, if we take the subjet analysis at face value [41]. The measurement of g_{WWH} is a little less precise than naively expected, given the weak-boson-fusion signatures including ample information on this coupling. Comparing the results for the two luminosities we see that the limiting factor for the WWH coupling is the statistics of the weak-boson-fusion channels. For the gluon-fusion production process combined with a decay $H \to WW$ we know that the kind of off-shell decay appearing for light Higgs masses is essentially impossible to extract from the sizable backgrounds.

Comparing the left and right set of panels, we see that in the Bayesian probabilities volume effects completely hide any kind of sign preference which might come out of the interference in the effective $g_{\gamma\gamma H}$ and g_{ggH}.

To highlight the importance of two-dimensional correlations, we show an extended set of them in figure 2. In contrast to the correlations shown in figure 1 these are not induced by effective couplings, i.e. through quantum effects, but purely based on the $(\sigma \cdot \mathrm{BR})$ structure our LHC measurements.

First of all, there will be a general correlation between all couplings. Similar to scaling the total width as described in section 3 we can shift the bottom Yukawa couplings which dominates the total Higgs width in the denominator of all rate measurements. We can compensate for such a shift by simultaneously scaling all relevant couplings, which gives a general tendency of a positive correlation of all couplings in this analysis.

The correlation between g_{WWH} and $g_{\tau\tau H}$ is induced by the two weak-boson-fusion
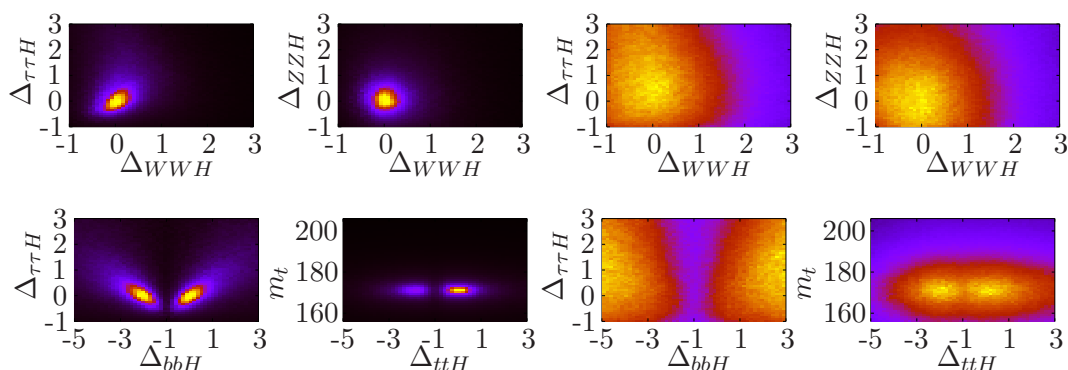
Figure 2. Correlations in profile likelihoods (left) and Bayesian probabilities (right), not allowing additional effective couplings. All experimental and theory errors included for low-luminosity running.

signatures, where from the same production process we can observe both decays at the LHC. This means, that the ratio $g_{WWH}/g_{\tau\tau H}$ is well constrained, without the possibility of compensating a shift of only one of the two decay couplings with another shift in the production cross section. This adds to the positive diagonal correlation $g_{WWH} \propto g_{\tau\tau H}$ in the profile likelihood panel in figure 2. There will be a slight distortion due to the fact that we can keep the weak-boson-fusion $H \to \tau\tau$ rate constant with a negative correlation $g_{WWH} \propto 1/g_{\tau\tau H}$.

The correlation between g_{WWH} and g_{ZZH} is less pronounced, mostly due to low statistics. In the weak-boson-fusion production process, the ZZ fusion channel typically accounts for $\mathcal{O}(25\%)$ of all signal events. Hence, we expect a fairly flat negative correlation between the two couplings. In the gluon-fusion production channel (and to some degree in the weak-boson-fusion channel) we can observe both decays to heavy gauge bosons, which means that the ratio of the two couplings protect the ratio of the two branching ratios. These two effects together with the general positive correlation described above again pull the $g_{WWH} - g_{ZZH}$ correlation into opposite directions and largely cancel. This is confirmed by figure 9 where the quality of the g_{bbH} extraction is reduced and the positive correlation becomes dominant.

In the third panel we show the correlation of the Yukawa couplings g_{bbH} and $g_{\tau\tau H}$, i.e. the ratio of the two down-type Yukawas. In many models, like in type-II 2HDM this ratio will be invariant under leading modifications for example by an additional factor $\tan\beta$. For LHC measurements, these two Yukawas are not directly linked, if we neglect the two numerically marginal contributions to $g_{\gamma\gamma H}$. However, we see the over-all scaling of all couplings also between these two.

Last, but not least we show the correlation between the top Yukawa coupling and the on-shell top mass. The latter we can measure at the LHC to $\mathcal{O}(1\,\text{GeV})$ and is already measured at the Tevatron to $1.2\,\text{GeV}$ [70]. We see that at this level a possible correlation of the top Yukawa coupling in the numerator of the effective gluon-Higgs coupling and the loop suppression by the top mass plays hardly any role.
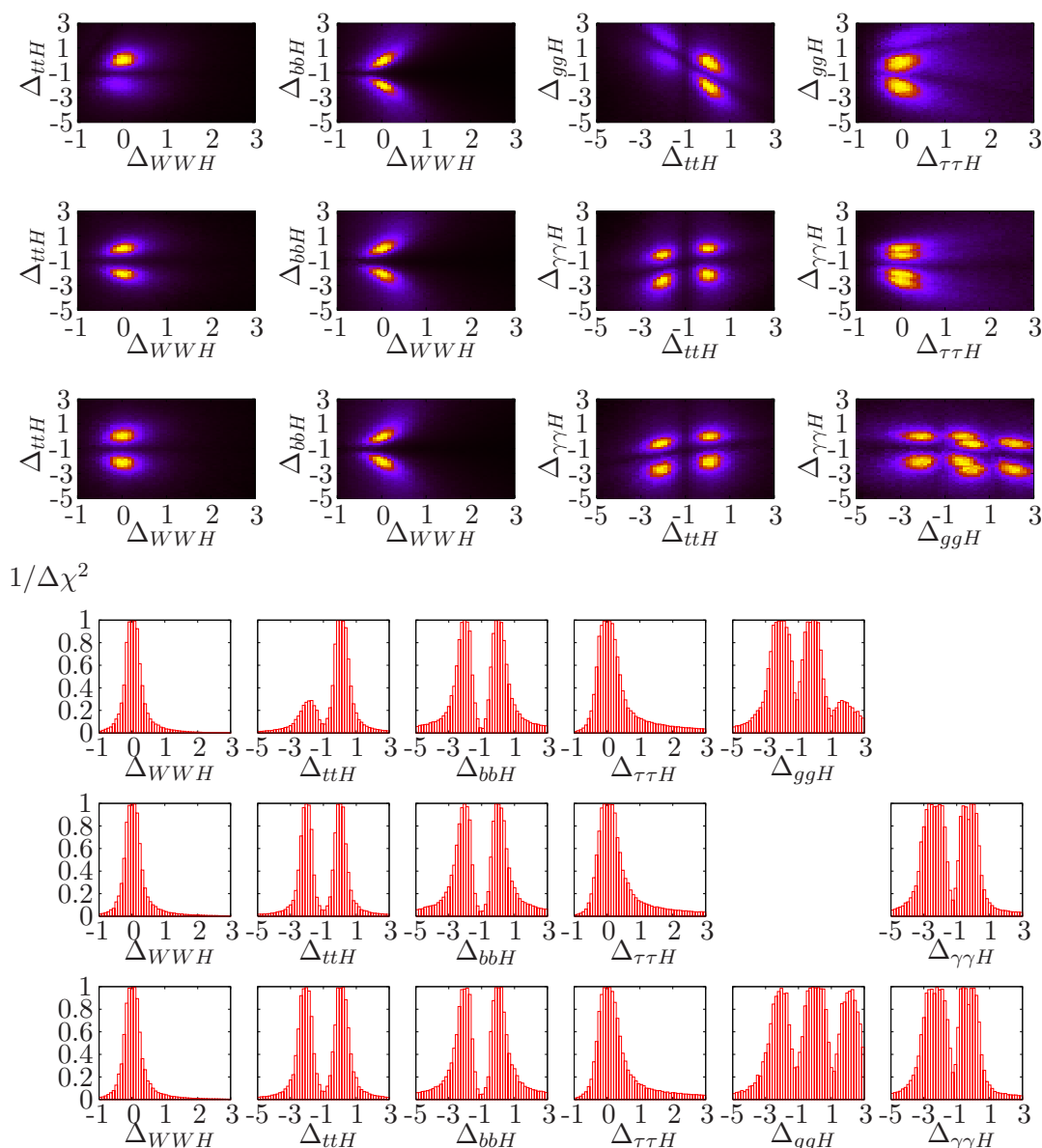
Figure 3. Profile likelihoods; the three rows correspond to (1) only a ggH effective coupling, (2) only a $\gamma\gamma H$ effective coupling, and (3) both of them. The corresponding results without any effective coupling are shown in figure 1.

Based on figures 1 and 2 we can already conclude that for this kind of analysis Bayesian probabilities are less useful to understand the correlations around the best-fit parameter points and that alternative global maxima will likely not play a big role in our analysis. Therefore, for the rest of this paper we limit ourselves to (cooling) profile likelihoods.

In figure 3 we study in detail the impact of the additional effective g_{ggH} and $g_{\gamma\gamma H}$. Both of them appear in the Standard Model, but they are completely described by the tree-level g_{ttH} and g_{WWH} couplings, with minor contributions from the bottom quark loop. Physics

beyond the Standard Model will always appear in these loops, in weakly interacting as well as in strongly interacting models.

We start from the discussion of figure 1 which indicates that without effective couplings there is a clear correlation between g_{ttH} and g_{WWH}, which are the two loops contributing to the one-loop $H\gamma\gamma$ coupling. The question is what happens if we allow for an additional effective coupling as shown in eq. (3.2). In the Standard Model, such small couplings exist, and in a general TeV-scale physics model they can become strong. In figure 3 we first add an additional g_{ggH}. This is at the expense of one of the measurements of the top Yukawa, since the dimension-five ggH operator in the gluon-fusion production cross section is the main source of the g_{ttH} measurement. This is confirmed by their correlation or anti-correlation, depending on the sign of the top Yukawa. Both signs of g_{ttH} are in principle allowed, but their degeneracy is broken by the $\gamma\gamma H$ coupling. Since the sign of the sub-leading bottom Yukawa couplings is poorly constrained this implies that little changes as long as the top Yukawa couplings is still determined by the $g_{\gamma\gamma H}$. The correlation between g_{ggH} and $g_{\tau\tau H}$ we show as an example how these correlations are fed through the parameter space, combining the effects of loop contributions and production and decay rates.

Adding only an effective $g_{\gamma\gamma H}$ immediately allows for an equally likely negative top Yukawa coupling. Again, we see a weak correlation between $g_{\gamma\gamma H}$ and the top Yukawa, but since the latter is well determined through g_{ggH} it is quantitatively less relevant. We also see a correlation between $g_{\gamma\gamma H}$ and $g_{\tau\tau H}$, with four equally likely branches representing the two possible signs of g_{ttH} combined with the modulo-two degeneracy of $\Delta_{\gamma\gamma H} = -2$ or zero.

Finally, we allow for both effective couplings. The correlation between both effective couplings now shows eight distinct maxima, with modulo-two steps in Δ_{ggH} and $\Delta_{\gamma\gamma H}$ and a sign switch of the top Yukawa coupling. The left pair of solutions in the g_{ggH}–$g_{\gamma\gamma H}$ correlation has a (correct) positive top Yukawa coupling and a shifted $\Delta_{ggH} \sim -2$. The central two pairs include the Standard Model solution with positive top Yukawa and $\Delta_{ggH} \sim 0$ as well as a negative top Yukawa coupling combined with $\Delta_{ggH} \sim 0$. In the right pair the negative top Yukawa coupling is compensated by $\Delta_{ggH} \sim 2$. The same features we see in the one-dimensional likelihood for the effective Higgs-gluon coupling. Note that these solutions are only degenerate because the general effective couplings remove any sensitivity on the signs of the different Higgs couplings — confirming that the sign-flip symmetry is only broken by interferences in the loop couplings.

4.2 Theory errors

In general, to compare different hypotheses with data the central values of a parameter fit are useless without appropriate error bars. Therefore, also in this Higgs sector analysis we have to ensure that the error treatment is correct and that we understand the impact of different errors.

While the proper treatment of statistical and (correlated) systematic experimental errors is well established and standard in all analyses, the treatment of theory errors deserves a closer look. In figure 4 we compare the impact of theory errors on the (hypothetical) most constraining scenario we can imagine: a parameter set without effective couplings and assuming a full 300 fb^{-1} of integrated luminosity. Obviously, we expect theory errors
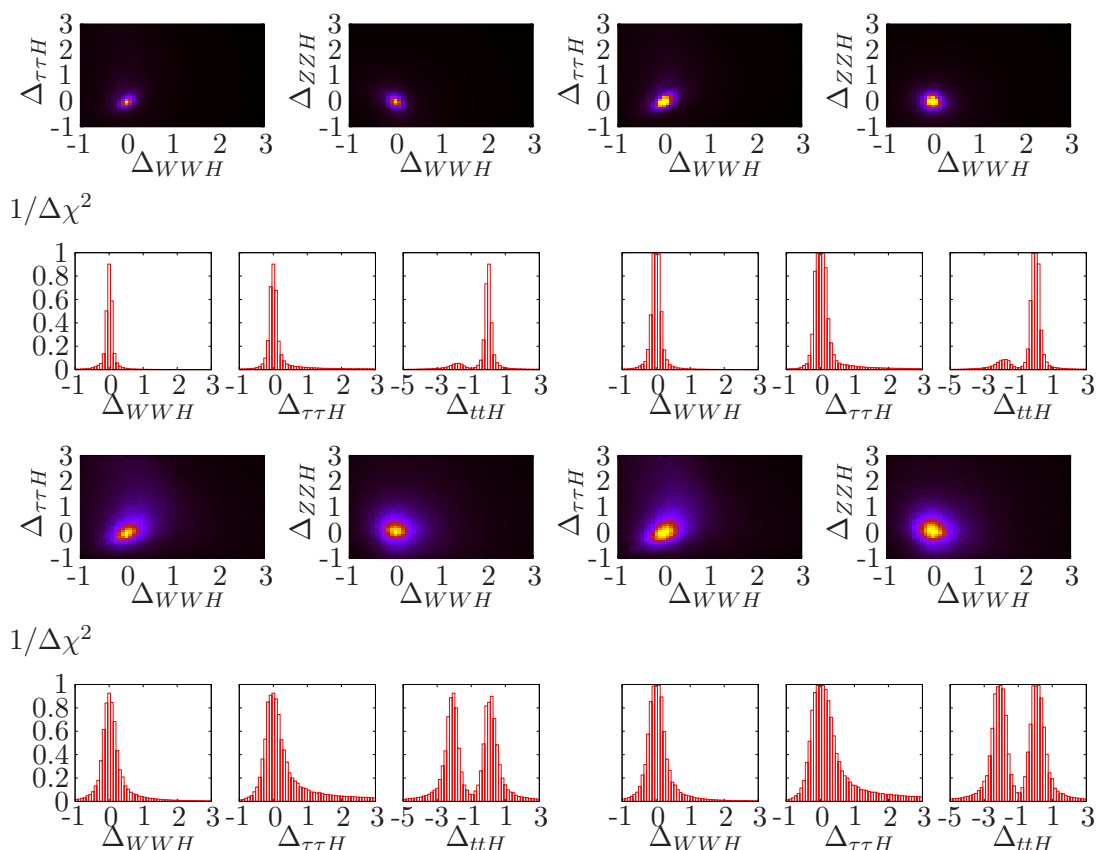
Figure 4. Profile likelihoods without (left) and including (right) theory errors. The top rows assume 300 fb^{-1} and no effective couplings, the bottom rows 30 fb^{-1} and both effective ggH and $\gamma\gamma H$ couplings.

to have a sizable effect on the results. The second scenario for which we study the effect of theory errors includes both effective couplings and a lower luminosity of 30 fb^{-1}. As discussed in section 4.1, including the two additional effective couplings has a strong effect on correlations and on alternative minima.

Including theory errors on the right-hand side we clearly see the flat region with maximum log-likelihood around the correct central value spanning a few bins. This is a direct consequence of the Rfit scheme. For each measurement there is a flat region around the central value with the size of the corresponding theory error and likelihood one. This multi-dimensional box translates into a region in parameter space, i.e. we can slightly vary each parameter around its central value without any penalty in the likelihood. Outside this flat region the curves should not drop equally fast in both cases. This is indeed visible, in particular for the 30 fb^{-1} case where the fall-off is not as steep as for 300 fb^{-1}. For example the tail for large $g_{\tau\tau H}$ looks exactly the same. It is interesting to note that theory errors also increase the likelihood of the alternative solution $\Delta_{ttH} = -2$ for forbidden effective couplings. This alters the effective coupling of the Higgs to photons which within theory errors we can slightly shift without increasing χ^2.
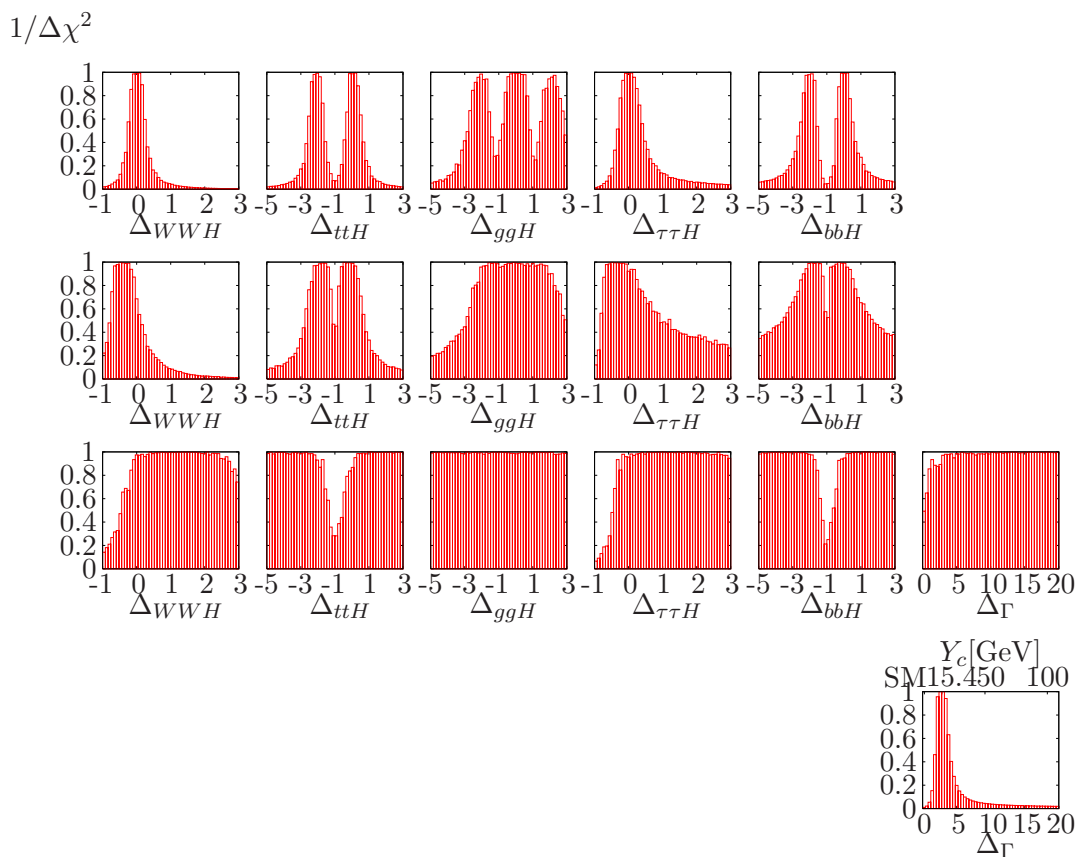
Figure 5. Profile likelihoods for the standard analysis (top row, copied from figure 1), an increased ccH coupling with no additional contribution to the Higgs width (second row), an increased ccH coupling and a scaling factor for the total width (third row), and finally this scaling factor only (single bottom panel). All experimental and theory errors included for low-luminosity running.

Theory errors can affect background predictions in addition to signal rates. However, most of the LHC Higgs searches rely on control regions or side bins. The classical example is the two-sided side bins in the $H \to \gamma\gamma$ search where the theory error does not have to account for higher-order corrections of the background rate. Therefore, we neglect the effect of background theory errors. The systematic errors on background rates are listed in table 2.

4.3 Unobserved or invisible?

There are two kinds of Higgs decays which we have not yet considered in this analysis. First, the Higgs boson can decay into invisible particles, like dark-matter agents, which would appear as missing transverse energy in the detector. As discussed in the introduction we skip this kind of analysis.

What is more interesting is an actually unobservable Higgs decay, i.e. a Higgs decay which at the LHC we could not see. Looking at the particle content of the Standard Model, any decay into light leptons would be immediately visible. Shifted couplings to

third-generation fermions are already part of our parameter set, as is the coupling to gluons and the electroweak gauge bosons. One thing that could still happen are Higgs decays to light quarks, which would completely vanish in the QCD continuum.

As an example, we consider an increase of the charm Yukawa coupling to 15.4 GeV, which corresponds to a branching ratio of roughly 80%. To be consistent, we also include this coupling in the rate for inclusive Higgs production. Identifying the light-jet coupling with the charm Yukawa is conservative in the sense that it minimizes the production rate for a given light-jet partial width because of the small charm parton densities.

In the parameter extraction, the first effect of this additional coupling is the increase of the inclusive production rate. This effect is stronger than suggested by just comparing g_{ggH} and g_{ccH}, because the latter induces a tree-level decay. This rate enhancement can be counter balanced by reducing the branching ratios, i.e. by reducing all relevant Higgs couplings to final-state particles. This implies very small rates from weak boson fusion, driving them deep into the Poisson region for 30 fb^{-1}. The effect on the parameter extraction we see in figure 5: in the second row the most likely points of all couplings are shifted by roughly the same amount. In addition, the errors are increased significantly, in particular for $g_{\tau\tau H}$. The separate peaks for g_{ggH}, corresponding to the different signs of the individual couplings, get smeared out into a large band of possible solutions.

The consequence of such a result should be a more careful analysis, now including a free Higgs width. Such a shift shown in eq. (3.4) can be implemented as a decay to an unobservable new-physics particle which does not appear inside the proton. Known examples for such effects are unobservable four-body Higgs decays [71]: The result we show in the third row of figure 5. We always find a best-fitting parameter point and the error bars are hugely inflated, in particular to large couplings. For the Standard Model couplings only the region around $\Delta = -1$, where the coupling vanishes, is excluded. The smallest possible solution we obtain when the additional contribution to the width is zero. In that case we reproduce the slope from the no-additional-contribution scenario, modulo statistics effects. The region of large couplings is similar to the scaling of a free total Higgs width discussed in section 3. Any increase can be compensated by a corresponding increase of the invisible decay mode. The predictivity of such an analysis is therefore rather limited.

There is a second scenario we can test at this stage: if there appears to be a problem with the total width we can fix all Standard Model couplings to their respective nominal values and only allow for an additional experimentally unobservable decay mode. This leads to a very simple one-dimensional analysis, where only Δ_Γ is varied. Technically, we identify this increase with a large ccH coupling, but without including its contribution to the Higgs production rate. Under this assumption we can determine the size of the additional contribution to the width, as shown in the bottom line of figure 5.

Finally, there is a third way to establish an upper bound on additional contributions to the Higgs width. Following the previous subsection we cannot simply add an additional contribution to the total width, because this would eliminate the possibility of determining the absolute scale of the couplings. On the other hand, following the argument in section 3 we can trade the assumption on the Higgs width for a limit in any other coupling, for example fixing g_{WWH} to its Standard Model value. As we will see in section 5.2 this is

$1/\Delta\chi^2$
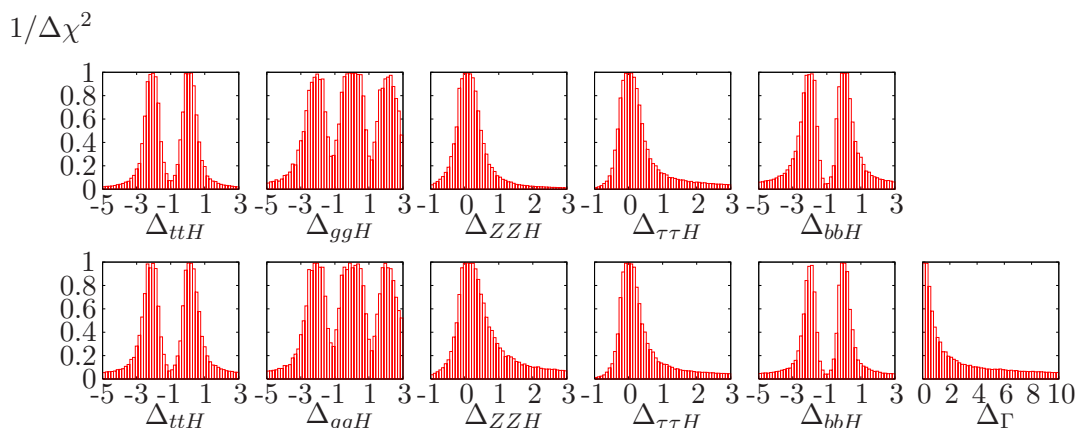
Figure 6. Profile likelihoods for the standard parameter analysis (top row, copied from figure 1), and an additional contribution to the total width while at the same time keeping g_{WWH} fixed to its Standard model value (bottom rows). All experimental and theory errors included for low-luminosity running.

the best-determined coupling of the parameter set. In models with more than one doublet this means that we either assume a rapid decoupling of the additional heavy states or close enough Higgs modes that we cannot resolve them in the transverse mass reconstruction of the WW final state [72].

In figure 6 we see that this indeed retains well-defined solutions. The errors on the different parameters stay at a similar level as the original analysis, with g_{bbH} and $g_{\tau\tau H}$ being measured mildly more precisely. Both of them are determined in channels with a production-side g_{WWH}. The impact of the Z boson replacing the W in these channels is always sub-leading. The additional coupling ranges around zero with a standard deviation of roughly twice the Standard-Model width. This error corresponds to the error in the bottom Yukawa coupling, which is the main observable partial width and well determined.

The results for these different scenarios give us some confidence in the robustness of our weak-scale analysis. While the LHC cannot make any direct statement about the total Higgs width (as discussed in section 3), effects from unobserved decays or shortcomings of our effective Lagrangian hypothesis will surface as unexplained effects in the parameter extraction. These effects then trigger for example modifications of our ansatz and can be studied.

4.4 Coupling ratios

Given the sizable correlations in the Higgs-sector parameter space we could try to define better-suited parameters than individual Higgs couplings. In a way, this is in analogy to the extraction of supersymmetric masses from cascade decays, where we can extract mass differences much more precisely than the actual masses. In the Higgs sector the hope is that ratios of couplings are better suited for an extraction from LHC measurements, for example coming from different decays but the same production process (or vice versa) [10, 11]. In this situation some of the systematic and theory errors will cancel. The same trick allows us
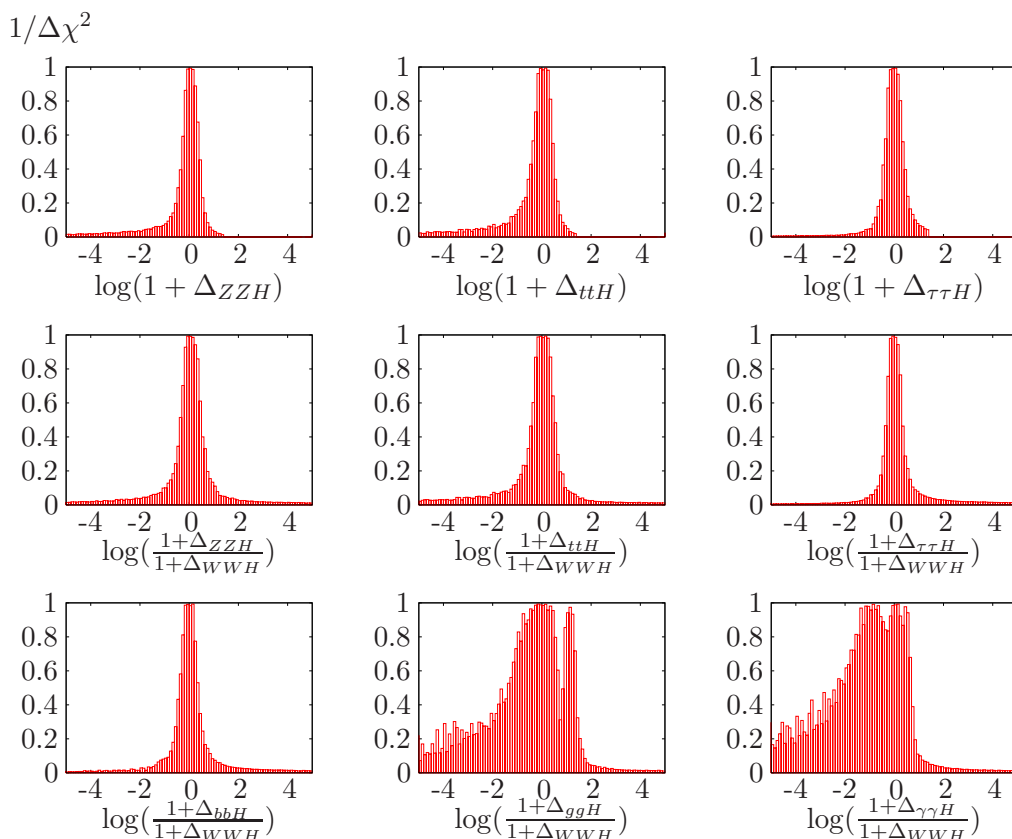
Figure 7. Profile likelihoods for the absolute couplings (top row, same input as in figure 3), for the logarithm of the ratio of the g_{ZZH}, g_{ttH}, $g_{\tau\tau H}$ (center row, left to right), g_{bbH}, g_{ggH} and $g_{\gamma\gamma H}$ (bottom row, left to right) couplings and the g_{WWH} coupling. All couplings/ratios are normalized to their Standard Model value. We include all experimental and theory errors for a running of 30 fb^{-1}.

to extract flavor-physics limits from data in the presence of large uncertainties in low-energy QCD predictions or form factors.

In general, we might expect for example coupling ratios of $1/2$ and 2 to be symmetric and equally likely. However, naively showing the coupling ratio would tilt this distribution, so in figure 7 we instead show the logarithms of the absolute values of coupling ratios, normalized to their respective Standard Model values; g_{WWH} serves as the general normalization. For the couplings present in the Standard Model we see the expected peak around zero. The secondary solution of $\Delta_{ttH} = -2$ also gets mapped to zero by our formulas for the ratios. For the effective couplings g_{ggH} and $g_{\gamma\gamma H}$ we see secondary peaks, originating from the alternative solutions in figure 3. For the ggH coupling both the peaks at $\Delta_{ggH} = 0$ and -2, where the latter corresponds to a top coupling with the correct sign and over-compensation by the effective coupling, appear at zero. The peak at $\Delta_{ggH} = 2$, compensating for a negative top coupling, appears just above one for the logarithmic ratio. In the $\gamma\gamma H$ case we see in principle the same effects. As the top-quark contribution is sub-leading we now have four solutions. They appear as three different peaks in the logarithmic ratio, because again $\Delta_{\gamma\gamma H} = 0$ and -2 coincide at zero deviation.

Both effective couplings also show a softer shoulder below the peak than above. The same effect we see for g_{ZZH} and g_{ttH}, albeit less pronounced. This is due to the fact that reducing the couplings gives us a well-defined worst case of zero coupling, i.e. no signal events. In contrast, increasing a coupling we can generate arbitrarily large numbers of events with an arbitrarily small inverse likelihood.

To answer the crucial question, we show the coupling constants itself in the top row of figure 7. For g_{ZZH} we see hardly any difference between the coupling and the coupling ratio. The main measurement of this coupling arises from the gluon-fusion initial state where W bosons do not play any role. For g_{ttH} the situation is similar; both, g_{ttH} and g_{WWH} are determined from a multitude of measurements so there is no particular benefit in looking at this ratio. In contrast, for $g_{\tau\tau H}$ we can determine the ratio more precisely than the absolute coupling, because of the two final states in weak-boson-fusion production. The most striking improvement we find for g_{bbH}, where we exploit the correlation between the different occurrences of g_{WWH} and the total width, dominated by bottom decays. The detailed discussion of errors on the ratios we defer to section 5.2; it will give us an improvement on the extraction of typically roughly $\sim 10\%$.

5 Higgs couplings

Before we can start determining the errors on the Higgs-sector parameters given a complete simulated data set at the LHC, we have one final step to implement. Until now, we have always tested our model on a set of perfect measurements, i.e. these measurements sit on their central value as predicted by the Standard Model without any smearing. As long as we do not extract error bars from such a data set this assumption is safe. However, for the final word on errors we need to move the signal and background rates away from the central value simulating an expected statistical fluctuation.

5.1 Smearing the data

One- and two-dimensional profile likelihoods for the Higgs parameter extracted from a smeared set of measurements we show in figure 8. This smearing of the one pseudo-measurement includes all experimental but no theory errors. We see that the behavior of our results does not change significantly whether we use the true or smeared data set. The best-fitting points are slightly shifted away from the correct Standard-Model values. Moreover, the peak structures get broader, as the different measurements now attempt to pull the parameters into different directions. This indicates that any kind of error estimate from these likelihood distributions has to be taken with a grain of salt and we better rely on toy experiments [8] to extract reliable error bars for the model parameters.

In table 4 we list the five best-fitting parameter points, obtained from an additional Minuit run starting from the best points of our (weighted and cooling) Markov chains. The first point is the closest to the Standard Model, where all couplings have the correct sign. All alternative solutions appear after flipping the sign of one or several of the couplings via $\Delta = -2$. Only in the $\gamma\gamma H$ effective coupling, where the W and the top interfere destructively does the sign play a role. In the second column the sign of the two effective
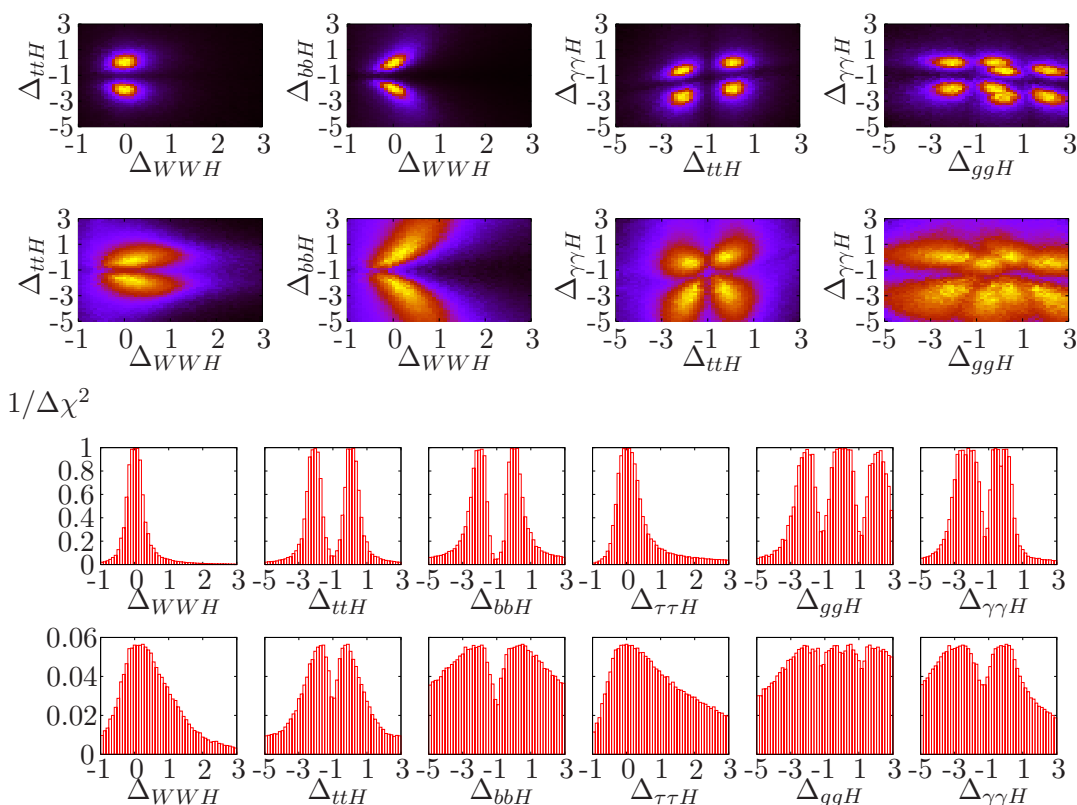
Figure 8. Profile likelihoods for unsmeared (top, taken from figure 3) and smeared (bottom) measurements assuming 30 fb^{-1}. We include both experimental and theory errors in our analysis.

	best solutions				
Δ_{WWH}	0.12	0.11	0.11	0.09	0.09
Δ_{ZZH}	0.12	0.13	0.11	0.10	0.09
Δ_{ttH}	-0.29	-0.29	-0.30	-1.70	-1.70
Δ_{bbH}	0.17	0.16	-2.15	-2.12	-2.11
$\Delta_{\tau\tau H}$	0.02	0.03	0.03	-0.10	-0.10
$\Delta_{\gamma\gamma H}$	-0.01	-2.43	-2.42	-0.38	-2.76
Δ_{ggH}	0.47	-1.85	0.34	-0.48	-0.47

Table 4. Best solutions for one (experimentally) smeared data set with 30 fb^{-1}. The Higgs mass is 120 GeV. Both experimental and theory errors included.

couplings is changed. The additional contributions to the effective couplings just over-compensate the Standard-Model parts. In the third column the bottom Yukawa coupling has a negative sign and this is reflected in a slight decrease in the effective gluon coupling. When we flip the signs from both the top and bottom quark in column four the ggH contribution is back to its original absolute value. In addition, we see the shift in the effective photon coupling, which has to compensate for the now constructive interference of the W and t loops. The same shift appears in the fifth column where the effective photon

	no effective couplings				with effective couplings			
	RMS	σ_{symm}	σ_{neg}	σ_{pos}	RMS	σ_{symm}	σ_{neg}	σ_{pos}
m_H	± 0.36	± 0.26	-0.26	$+0.26$	± 0.38	± 0.25	-0.26	$+0.25$
Δ_{WWH}	± 0.31	± 0.23	-0.21	$+0.26$	± 0.29	± 0.24	-0.21	$+0.27$
Δ_{ZZH}	± 0.49	± 0.36	-0.40	$+0.35$	± 0.46	± 0.31	-0.35	$+0.29$
Δ_{ttH}	± 0.58	± 0.41	-0.37	$+0.45$	± 0.59	± 0.53	-0.65	$+0.43$
Δ_{bbH}	± 0.53	± 0.45	-0.33	$+0.56$	± 0.64	± 0.44	-0.30	$+0.59$
$\Delta_{\tau\tau H}$	± 0.47	± 0.33	-0.21	$+0.46$	± 0.57	± 0.31	-0.19	$+0.46$
$\Delta_{\gamma\gamma H}$	—	—	—	—	± 0.55	± 0.31	-0.30	$+0.33$
Δ_{ggH}	—	—	—	—	± 0.80	± 0.61	-0.59	$+0.62$
m_b	± 0.073	± 0.071	-0.071	$+0.071$	± 0.070	± 0.071	-0.071	$+0.072$
m_t	± 1.99	± 1.00	-1.03	$+0.98$	± 1.99	± 0.99	-1.00	$+0.98$

Table 5. Errors on the measurements from 10000 toy experiments. We quote errors for Standard Model couplings only and including effective ggH and $\gamma\gamma H$ couplings using 30 fb^{-1} of integrated luminosity. The different σ measures are defined in the text.

	no effective couplings			with effective couplings		
	σ_{symm}	σ_{neg}	σ_{pos}	σ_{symm}	σ_{neg}	σ_{pos}
$\Delta_{ZZH/WWH}$	± 0.46	-0.36	$+0.53$	± 0.41	-0.40	$+0.41$
$\Delta_{ttH/WWH}$	± 0.30	-0.27	$+0.32$	± 0.51	-0.54	$+0.48$
$\Delta_{bbH/WWH}$	± 0.28	-0.24	$+0.32$	± 0.31	-0.24	$+0.38$
$\Delta_{\tau\tau H/WWH}$	± 0.25	-0.18	$+0.33$	± 0.28	-0.16	$+0.40$
$\Delta_{\gamma\gamma H/WWH}$	—	—	—	± 0.30	-0.27	$+0.33$
$\Delta_{ggH/WWH}$	—	—	—	± 0.61	-0.71	$+0.46$

Table 6. Errors on the ratio of couplings for a 120 GeV Higgs, corresponding to table 5. The coupling ratio is normalized to the Standard Model value according to eq. (5.1). For the Standard Model dataset used in this study the central value of $\Delta_{jjH/WWH}$ is zero, therefore only the errors are quoted.

coupling over-compensates the Standard-Model contributions.

Note that none of these solutions are 'true' alternative solutions, i.e. minima in χ^2 not correlated to the best-fit values and with a distinctly different underlying set of model parameters. This by hindsight justifies our choice of profile likelihoods for this analysis, as compared to Bayesian probabilities. Practically it also means that for the remaining part of this paper we focus on the 'most physical' parameter point, i.e. we ignore secondary points with $\Delta_{jjH} \sim -2$.

5.2 Best fit with error bars

In table 5 we show the errors on the extraction of Higgs coupling parameters. These errors we obtain from 10000 toy experiments, each smeared around the true data point including all experimental and theory errors. Besides calculating a root-mean-square error, we histogram the best fits for each parameter and extract σ_{symm} using a Gaussian fit. As we do not expect the errors to be symmetric, we also fit a combination of two Gaussians with the same maximum and the same value at the maximum, but different widths. Depending on whether we are below or above the maximum we use the first (σ_{neg}) or the second

Gaussian (σ_{pos}). For Δ_{ZZH} we see that as we approach -1, or vanishing coupling, the histogram goes to a constant value and is not well-fitted by a Gaussian. Therefore, for the lower branch of this coupling we fit only the central part within one standard deviation. Using a different measure for the shape of the error distribution we also show the standard RMS values for all couplings. They are systematically larger, owed to individual toy experiments far from the best-fit points. Only for symmetric Gaussian behavior we can expect these three error measures to coincide.

First, we see that a correlation between the mass measurements and the couplings plays hardly any role. The errors on the Higgs mass are symmetric and the values correspond to our input data.

A bit surprisingly, g_{WWH} is basically unchanged whether we allow effective couplings or not. This coupling is the main contribution to the effective $g_{\gamma\gamma H}$, so we would expect that allowing for additional effective coupling should remove the decay to photons from the g_{WWH} determination. The results indicate that the accuracy from the remaining measurements is sufficient to determine g_{WWH}.

For the ttH coupling the situation is different. Besides its small tree-level impact it is the dominating contribution to g_{ggH} and a sub-leading contribution to $g_{\gamma\gamma H}$. Hence, allowing effective couplings increases the errors. With and without effective couplings a Gaussian does not describe the errors accurately. In fact, including effective couplings we see a flat part around the Standard Model value, originating from our flat theory errors, and then a slightly steeper exponential fall-off.

The $\tau\tau H$ and bbH couplings are both strongly linked to g_{WWH}, because of their respective production modes. The $t\bar{t}$-associated production channel has too large errors to play a significant role. Consequently, we do not see any dependence on the existence of effective couplings.

The ZZH coupling shows a particular effect when we include the effective couplings; its error is decreased. Such a behavior is counter-intuitive, because naively we would expect that such an additional coupling can always be considered a nuisance parameter which we need to remove. No matter if we integrate it out or project it away, the resulting error should form some kind of envelope. However, the situation changes once we include correlations. Let us consider two couplings g_1 and g_2 (with a strong positive correlation) contributing to the same observable as $g_1^2 g_2^2$. With a combined shift the relative errors δ_1 and δ_2 on the couplings yield a total shift $g_1^2 g_2^2 (\delta_1 + \delta_2)$ on the observable, limited by the measurement. For example, if due to the positive correlation both terms in the parenthesis are strictly positive, the upper limit on the observable now splits into two contributions, one for each parameter. In contrast, if we fix $\delta g_1 = 0$ δg_2 alone accounts for the complete deviation in the observable.

The main source for determining g_{ZZH} is gluon-fusion production with subsequent Higgs decay into two Z. Without any effective couplings only the top Yukawa coupling determines the production rate, which is constrained by many other measurements. To account for the measured event rate we need to adjust g_{ZZH} accordingly. With additional contributions to g_{ggH} the top Yukawa coupling becomes largely irrelevant and the production and decay couplings of the $gg \to H \to ZZ$ channel form exactly the combination

discussed above. From section 4.1 we know that they are positively correlated, so indeed the error on Δ_{ZZH} can decrease.

In table 6 we show the errors on $\Delta_{jjH/WWH}$, defined in the following equation as the deviation from 1 of the ratios of the coupling constants to the WWH coupling normalized to the Standard Model value:

$$\frac{g_{jjH}}{g_{WWH}} \longrightarrow \left(\frac{g_{jjH}}{g_{WWH}}\right)^{\text{SM}} \left(1 + \Delta_{jjH/WWH}\right) \tag{5.1}$$

A non-zero central value for $\Delta_{jjH/WWH}$ would arise in new physics scenarios. Thus $\Delta_{jjH/WWH}$ provides information on a possible shift of the coupling ratios as well as the error on the coupling ratio. The central value of $\Delta_{jjH/WWH}$ is zero for the Standard Model dataset used in this study, therefore we discuss only the errors on $\Delta_{jjH/WWH}$.

Table 6 confirms the qualitative results from the profile likelihoods in section 4.4. The error on g_{ZZH} even increases once we form the ratio. The main determination mode is via the gluon-fusion initial state, which is independent of g_{WWH}. An additional constraint enters via the subleading contribution to weak boson fusion, where g_{WWH} and g_{ZZH} occur additively, so forming the ratio exacerbates deviations instead of decreasing them. For the top-quark coupling the effect of the effective photon coupling becomes clearly visible. Without this additional parameter g_{ttH} and g_{WWH} are linked and consequently the error on the ratio is significantly smaller than the error on the coupling itself. The additional $g_{\gamma\gamma H}$ breaks this correlation and we no longer gain anything by using the ratio. For all other couplings we observe more or less significantly smaller errors for ratios of couplings, because the production-side g_{WWH} enters the determination of the decay-side couplings. Only the correlation between the well-measured g_{WWH} and g_{bbH} sticks out; it is due to the appearance of the total width in all rate predictions, which leads to strong correlations as discussed in section 4.1.

A note of caution should be added: the error on the error determination of the ratios of the coupling constants is non-zero. This is due to the fact that the coupling ratios have been determined from the coupling central values for a given toy experiment. Then for each toy experiment the ratio of the couplings calculated and the distribution of these ratios analyzed. The flat theory errors do not ensure a cancellation of correlated theory errors in these ratios. As the errors for the integrated luminosity of 30 fb^{-1} are dominated by the expected experimental error (78% to 94% of the total error as shown in table 1), we defer the development a more sophisticated treatment ensuring the full cancellation to a later date. We have checked however that by setting the theory errors to zero (implying a full cancellation of all errors) the error on the coupling ratios is improved by at most 10%.

5.3 Bottom Yukawa coupling

As mentioned in section 3 the measurement of the bottom Yukawa coupling is crucial to the success of this parameter analysis; without it we would hugely underestimate the total width of the Higgs boson and scale down all couplings correspondingly to obtain the measured production and decay rates. For a long time the LHC experiments expected the $t\bar{t}H$ production process to be best suited for Higgs decaying to bottoms. Such a complex
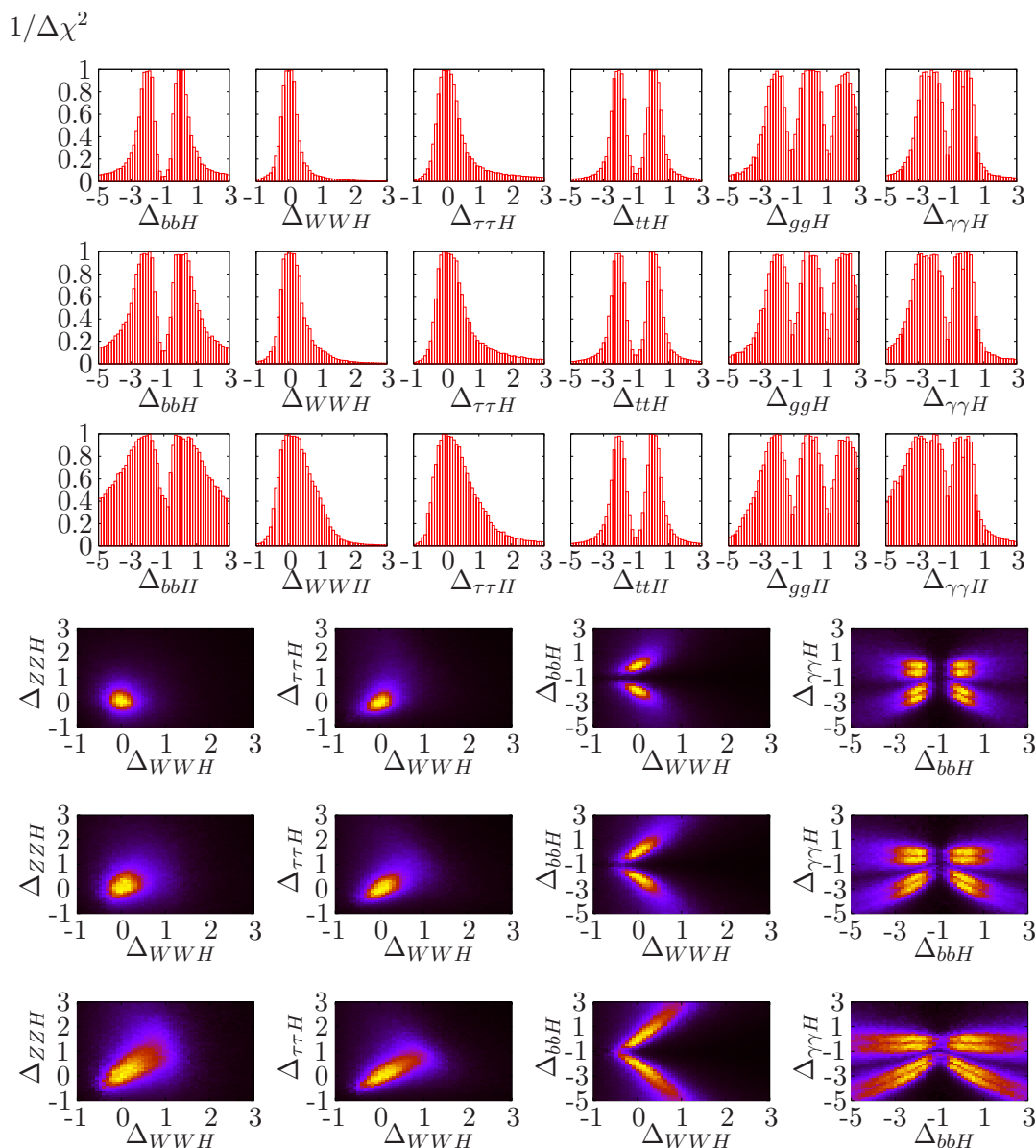
Figure 9. Profile likelihoods including the WH/ZH channel (upper row), WH/ZH with reduced sensitivity (center) and only $t\bar{t}H$ (lower) with a decay $H \to b\bar{b}$. All experimental and theory errors included for low-luminosity running (true data points).

signature is more promising than simply looking for inclusive $b\bar{b}$ production or weak-boson-fusion production, because it includes more information to reduce backgrounds. On the other hand, several bottom jets lead to combinatorial errors, which turn out to largely kill this signature. Recently, there has been progress in understanding the structure of bottom jets coming from a Higgs resonance as compared to continuum QCD production. These two sources can be distinguished using information from the merging of subjets inside the jet algorithm used. Triggering requires for example additional leptons in the final state,

which makes VH the preferred production channel. While these results have not yet been confirmed by detailed simulations, we nevertheless use them to illustrate the impact of the $H \to b\bar{b}$ channels on our analysis.

In figure 9 we first show results using the published $WH, H \to b\bar{b}$ results at face value. This is the signature we base our entire analysis on. To be consistent with the other channels, we use the rates as in ref. [41] but included our own systematic and theory errors.

In the second line we show results with a 50% reduced signal rate. As expected, all error bars are slightly increased, but the features of the distributions are virtually unchanged. Focusing on g_{bbH} we see that even with the reduced sensitivity a precise measurement is possible. The slight degradation of this coupling (and with it of the total width) then propagates into all remaining couplings.

Once we remove the WH/ZH subjet channel from our analysis a determination of the bottom Yukawa coupling becomes impossible. Its error bar extends to a continuum $\mathcal{O}(150\%)$ around the input value, and only a zero coupling is significantly less likely. The one measurement to determine g_{bbH} is top-quark-associated Higgs production. However, for this channel a measurement of zero events only requires a fluctuation of 0.7 standard deviations. An additional constraint enters via the total width, but we already know that there is a scaling symmetry. And finally, for the bottom contributions to the effective g_{ggH} and $g_{\gamma\gamma H}$ to play any role we need an enhancement of the bottom-Higgs coupling far beyond those considered here.

Aside from a broader peak structure of Δ_{bbH} we also observe considerably higher shoulders towards large values of the bottom Yukawa coupling. In this regime the branching ratio into bottom quarks gradually approaches one, so any increase in the coupling hardly shifts the number of $H \to b\bar{b}$ events. In the center of the Δ_{bbH} distribution the $\Delta\chi^2$ value for vanishing coupling ranges around 1.5 in the absence of the subjet analysis. The ttH channel cannot give such a large value, which means there is an additional indirect contribution from the total width.

Precisely due to the increased uncertainty on the total width the otherwise well determined g_{WWH} suffers visibly. Not surprisingly, this increased error bar immediately propagates into $g_{\tau\tau H}$ because of the correlated production process. In contrast, the top Yukawa coupling is virtually unchanged: first, the $t\bar{t}H$ production channel of bottom quarks contributes nothing to the top Yukawa measurement, and secondly the bottom contribution to g_{ggH} is small enough to still vanish in the error. The same is true for the effective g_{ggH} shown in figure 9. Both these couplings appear only on the production side of our measurements, so the bigger uncertainty on g_{bbH} will already be absorbed by the respective decay channel. The situation is different for the effective $g_{\gamma\gamma H}$, where the broader range of the Δ_{WWH} requires a larger variation of $\Delta_{\gamma\gamma H}$ to fulfill the constraints in particular from the well-measured inclusive $H \to \gamma\gamma$ channel.

As already alluded to in section 4.1, with most measurements significantly degraded we now observe the proper correlation between g_{WWH}, g_{ZZH} and $g_{\tau\tau H}$ from the weak-boson-fusion channels. Moreover, we see the positive correlation from the two observed decays in gluon fusion.

In table 7 we show errors on the parameters for the three different scenarios. Again we

	full measurements			reduced sensitivity			only $t\bar{t}H$, $H \to b\bar{b}$		
	σ_{symm}	σ_{neg}	σ_{pos}	σ_{symm}	σ_{neg}	σ_{pos}	σ_{symm}	σ_{neg}	σ_{pos}
Δ_{WWH}	$\pm\,0.24$	$-\,0.21$	$+\,0.27$	$\pm\,0.32$	$-\,0.25$	$+\,0.40$	$\pm\,0.33$	$-\,0.24$	$+\,0.43$
Δ_{ZZH}	$\pm\,0.31$	$-\,0.35$	$+\,0.29$	$\pm\,0.46$	$-\,0.49$	$+\,0.45$	$\pm\,0.59$	$-\,0.33$	$+\,0.64$
Δ_{ttH}	$\pm\,0.53$	$-\,0.65$	$+\,0.43$	$\pm\,0.54$	$-\,0.60$	$+\,0.50$	$\pm\,0.48$	$-\,0.56$	$+\,0.41$
Δ_{bbH}	$\pm\,0.44$	$-\,0.30$	$+\,0.59$	$\pm\,0.75$	$-\,0.64$	$+\,0.80$	$\pm\,0.78$	$-\,0.43$	$+\,0.84$
$\Delta_{\tau\tau H}$	$\pm\,0.31$	$-\,0.19$	$+\,0.46$	$\pm\,0.36$	$-\,0.18$	$+\,0.56$	$\pm\,0.39$	$-\,0.20$	$+\,0.60$
$\Delta_{\gamma\gamma H}$	$\pm\,0.31$	$-\,0.30$	$+\,0.33$	$\pm\,0.31$	$-\,0.31$	$+\,0.30$	$\pm\,0.33$	$-\,0.33$	$+\,0.33$
Δ_{ggH}	$\pm\,0.61$	$-\,0.59$	$+\,0.62$	$\pm\,0.59$	$-\,0.54$	$+\,0.64$	$\pm\,0.66$	$-\,0.48$	$+\,0.82$

Table 7. Errors on the measurements including the WH/ZH channel (left, from table 5), WH/ZH with reduced sensitivity (center) and only $t\bar{t}H, H \to b\bar{b}$ (right). We assume 30 fb^{-1} of integrated luminosity.
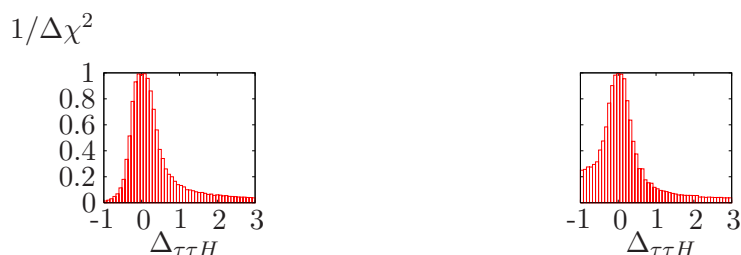
Figure 10. Profile likelihood for $\Delta_{\tau\tau H}$ including the standard error of 5% (left) and an increased error of 100% (right) on the central mini-jet veto. We show results for true data points and 30 fb^{-1}.

	5% error on minijet veto			100% error on minijet veto		
	σ_{symm}	σ_{neg}	σ_{pos}	σ_{symm}	σ_{neg}	σ_{pos}
Δ_{WWH}	$\pm\,0.24$	$-\,0.21$	$+\,0.27$	$\pm\,0.26$	$-\,0.29$	$+\,0.23$
Δ_{ZZH}	$\pm\,0.31$	$-\,0.35$	$+\,0.29$	$\pm\,0.32$	$-\,0.37$	$+\,0.30$
Δ_{ttH}	$\pm\,0.53$	$-\,0.65$	$+\,0.43$	$\pm\,0.55$	$-\,0.63$	$+\,0.49$
Δ_{bbH}	$\pm\,0.44$	$-\,0.30$	$+\,0.59$	$\pm\,0.47$	$-\,0.31$	$+\,0.64$
$\Delta_{\tau\tau H}$	$\pm\,0.31$	$-\,0.19$	$+\,0.46$	$\pm\,0.35$	$-\,0.33$	$+\,0.37$
$\Delta_{\gamma\gamma H}$	$\pm\,0.31$	$-\,0.30$	$+\,0.33$	$\pm\,0.37$	$-\,0.31$	$+\,0.43$
Δ_{ggH}	$\pm\,0.61$	$-\,0.59$	$+\,0.62$	$\pm\,0.61$	$-\,0.44$	$+\,0.75$

Table 8. Errors assuming the 5% standard error on the mini-jet veto (left, from table 5), and assuming an increased error of 100% (right), using 30 fb^{-1} of integrated luminosity.

fit only the central peak around the Standard Model solution. These numbers confirm the findings from figure 9. A very prominent shift we see of course in g_{bbH}, as this is directly affected by changes in the subjet analysis. There we also see a large fraction of solutions where the coupling vanishes. Other couplings are extracted with a reduced precision of $50 - 100\%$. Only the error on g_{ttH} is largely unchanged with remaining differences in part due to statistical fluctuations.

5.4 Minijet veto

One of the crucial ingredients to the weak-boson fusion production analyses is the central mini-jet veto [29]. The two tagging jets are emitted into the forward regions of the detector, while the central region stays free of jets. This behavior is reflected in the small next-to-leading order QCD corrections to this process [30, 77]. Typical backgrounds as well as gluon-fusion production involving two jets do not share this feature. How well Monte-Carlo simulations describe the mini-jet veto probability is not yet established. Without any claim of a useful range we increase the uncertainty on the mini-jet veto probability from 5% to clearly unrealistic 100%.

In table 8 we see that even with this huge theory error the numbers hardly change at all. The fit of a symmetric Gaussian to the toy experiments consistently enlarges the errors, although the effect is mostly minimal. The varying behavior for the asymmetric errors can be traced back to statistical fluctuations. Only for $g_{\tau\tau H}$ we see a significant change compared to our normal analysis. This coupling is determined exclusively via weak-boson-fusion channels, so an increase in the error directly affects this coupling. In figure 10 we see a clearly finite likelihood for vanishing coupling. In the complete scan we even see a slight peak in this place, because due to the large errors it is now possible that the rates for the weak-boson-fusion channels fluctuate below the background. To illustrate a non-negligible effect of the increased error: we see that while the zero-signal solution is clearly excluded in the standard case, we now cannot even reach a 95% confidence level assuming an integrated luminosity 30 fb^{-1}.

While this discussion seems to indicate that the exact knowledge of the minijet veto probabilities is not crucial to our analysis, there are two caveats: first of all, we only study the effect of the minijet veto probability for the signal, while we assume that it can be measured precisely for the backgrounds. This assumption might or might not be valid once we face real data. In particular in tough analyses like invisible Higgs searches (which we do not use in this analysis) this assumption needs to be reconsidered. Secondly, we limit ourselves to low-luminosity running, which hurts the statistical pull of the weak-boson-fusion channels. The moment we consider for example 100 fb^{-1} of data this situation will likely change.

6 Beyond the Standard Model

The main aim of the kind of Higgs sector analysis presented in this paper is to probe the nature of the Higgs sector in case that we only see a light scalar Higgs boson at the LHC. In this section we study the application of the Higgs parameter analysis and the ansatz described in section 3 on a supersymmetric Higgs sector. We restrict the analysis to the standard without additional observables [65].

This ultraviolet completion of the Standard Model has the advantage or disadvantage that it contains a the decoupling limit in which the LHC might quite realistically be left with a single light Higgs boson with very similar properties to its Standard-Model counter part. Such an outcome is predicted for fairly small values of $\tan\beta \lesssim 10$, where the Yukawa

	Δ_{WWH}	Δ_{ZZH}	Δ_{ttH}	Δ_{bbH}	$\Delta_{\tau\tau H}$	$\Delta_{\gamma\gamma H}$	Δ_{ggH}	m_H
true	-0.13	-0.13	-0.19	3.27	3.29	0.19	-0.28	120.0
errors	± 0.45	± 0.61	± 0.63	± 2.34	± 3.35	± 0.99	± 1.12	± 0.29
	-0.43	-0.99	-0.60	-3.68	-3.23	-0.70	-0.69	-0.29
	$+0.48$	$+0.52$	$+0.65$	$+1.52$	$+3.58$	$+1.30$	$+1.46$	$+0.30$

Table 9. Couplings for the SPS1a-inspired scenario. We give the true values of our input and the error bars assuming 10000 toy experiments and 30 fb^{-1} of data.

couplings of the heavy Higgs states are not sufficiently enhanced to warrant a direct observation. In this regime the only hope to see a heavy Higgs at the LHC might be an on-shell decay $H \to hh$ with a subsequent decay for example to $b\bar{b}\gamma\gamma$ [37]. On the other hand, for small $\tan\beta$ the decoupling limit is approached far less rapidly, so that a careful analysis of all couplings of an observed light Higgs state might reveal significant deviations from their Standard-Model values.

In this section we study two different scenarios: first, we choose a fairly low mass for the heavy CP-odd Higgs boson m_A, so that we are not too far in the decoupling regime. In a second part we consider a gluophobic Standard-Model like Higgs, i.e. the top loop in the effective ggH coupling is largely canceled by a corresponding stop loop [74]. Just like in section 4 we use true data points to disentangle the effects of the models from smearing. In addition, we use the same effective theory as described in section 3 without including new Higgs search channels in the decays of new states and without including loop effects from particles seen elsewhere in Atlas or CMS.

6.1 Supersymmetric Higgs

As a first step of this application we need to replace all Standard Model measurements with the respective rates for a supersymmetric parameter point based on SPS1a [75]. After evolving the original SPS1a parameters from the high scale to the low scale using SuSpect [76], we change $\tan\beta$ to 7, A_t to -1100 GeV and m_A to 151 GeV. For this parameter choice g_{WWH} and g_{ZZH} are significantly smaller than in the Standard Model. It also predicts a light CP-even Higgs mass of 120 GeV. The true values for all Higgs couplings we give in the first line of table 9. Comparing these deviations with the Standard Model error bands in table 5 we can guess that only g_{bbH} and $g_{\tau\tau H}$ will be useful individually, provided we can extract them in this scenario. While the couplings to gauge bosons are different in our supersymmetric scenario, their shifts with respect to the Standard Model values are all within their respective errors.

For the fairly small value of $\tan\beta$ the heavy Higgs bosons H, A and H^+ will not be observed at the LHC, and certainly not using 30 fb^{-1} of data. The question is: can we distinguish such a scenario from a Standard-Model Higgs sector just looking for a light Higgs boson [73]?

Strictly speaking, we should account for the extended particle content of supersymmetry with an increased theory error on the perturbative predictions of the production and decay rates. However, in most production channels the quantum effects of new states are mass suppressed and hence within the errors quoted in table 3 [77, 78]. With real LHC
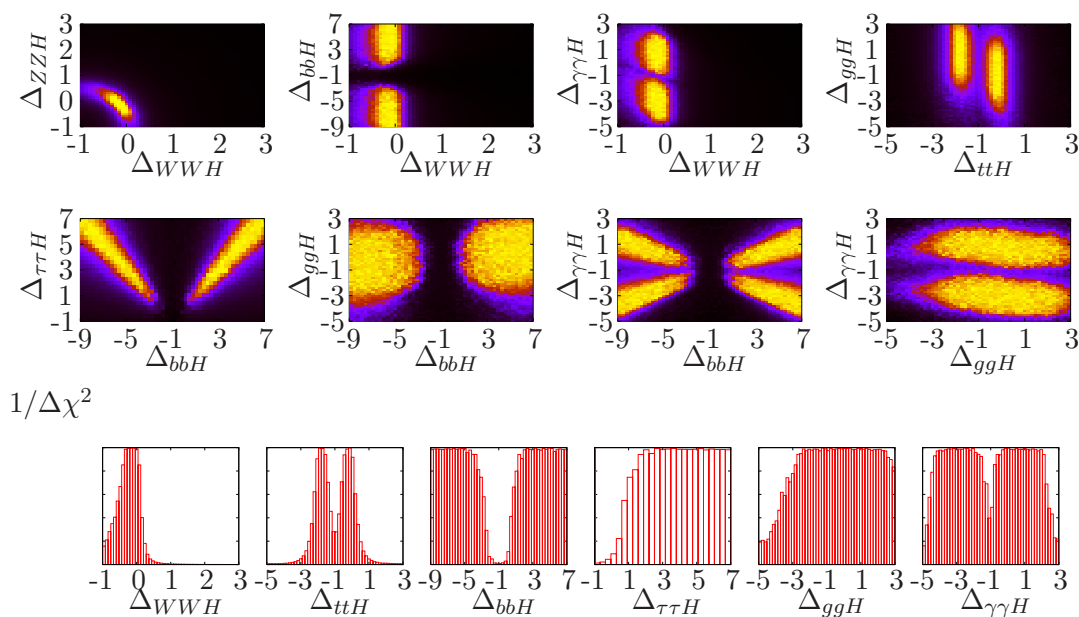
Figure 11. Profile likelihoods for the parameter point SPS1a with light m_A and modified A_t and $\tan\beta$ for 30 fb^{-1}. We include both experimental and theory errors in our analysis.

data this procedure would be an iterative process: first we would try to establish a deviation assuming the Standard Model particle content as the correct hypothesis. The general new-physics mass scale accounting for deviations from the Standard Model couplings will then feed back into our new physics analysis. In turn, taking information from other sectors into account we can refine the Higgs sector analysis.

In the first line of table 9 we can guess that essentially the four measurements with τ leptons or bottom quarks in the final state will contribute to our likelihood. All other measurements have too low production rates, even consistent with a null result with 30 fb^{-1}. We nevertheless include all measurements in our analysis for consistency. For the dominant measurements g_{ttH} g_{WWH} and g_{ZZH} appear on the production side. The latter is a sub-leading contribution to both weak boson fusion and the subjet analysis. For these four parameters we have four high-quality measurements, so we can hope to obtain a unique solution in this subspace when considering the complete set of measurements.

In the one-dimensional distributions in figure 11 we immediately see that the Standard Model hypothesis is not correct. For g_{bbH} we do not see an upper limit on the coupling strength. This is a consequence of the branching ratio into bottom quarks which event at unity would be compatible with the data. This limit removes any kind of rate measurement involving $H \to b\bar{b}$ from our measurements. The question remains if this leads to the free scaling of the total width with all couplings, as we have seen before.

In the subjet analysis channel we cannot make the branching ratio into bottom quarks larger than one, which induces a lower limit on g_{WWH}. On the other hand, we cannot decrease the branching ratio significantly, because this would require a large value of g_{WWH}.

Weak-boson-fusion production with subsequent decays into a pair of W bosons prohibits this solution, giving us an upper limit on g_{WWH} and inducing the lower limit on g_{bbH} in figure 11.

The same argument we can now apply to g_{ttH} and $t\bar{t}$-associated Higgs production. The lower limit on g_{bbH} induces an upper limit on g_{ttH}, which we also see in our results. Additional information we obtain from the non-observation of other channels with top-quark initial states. As this measurement is much less precise than the subjet analysis, the allowed values of the top-quark coupling extend further to positive values. The lower limit again reflects the fact that the bottom branching ratio cannot be larger than one.

The fourth parameter $\Delta_{\tau\tau H}$ is determined via weak boson fusion. The range in g_{WWH} implies an allowed range of branching ratios into a τ pair, and therefore of the ratio $g_{\tau\tau H}/g_{bbH}$ via the total width. Accordingly we see a strong positive correlation between these two couplings. This way, $g_{\tau\tau H}$ can extend to arbitrarily large values, while we have a definite lower limit and the Standard-Model value is clearly excluded.

For the remaining couplings we can extract limits from a non-observation in Higgs search channels. In $g_{\gamma\gamma H}$ we again see a scaling with the total width and therefore a strong correlation with g_{bbH}. The boundaries of $\Delta_{\gamma\gamma H}$ are simply given by our (arbitrary) limits on g_{bbH} in this scan, as we see in the correlation plot. The excluded region around -1 is a normalization effect: the WWH and ttH couplings contributing to the effective coupling are smaller than in the Standard Model, while our additional contribution is normalized to the Standard Model value. Setting $\Delta_{\gamma\gamma H} = -1$ would not give a vanishing total coupling but something too large. The bands we see are the regions where the additional contribution cancels the loop-induced coupling.

For the g_{ggH} coupling we do not see a scaling with g_{bbH}, because any effect of varying this coupling will already be compensated by the associated decay coupling. Including the $\tan\beta$ enhancement the bottom loop can now become large enough to give a relevant contribution to the effective coupling, so we then need to dial the additional parameter accordingly to cancel the combinations from both heavy quarks. Therefore, we do not see a sharp peak in Δ_{ggH} but a wide band of best-fitting points.

Given such a scenario where we see clear deviations from the Standard Model, the question arises at which level can we exclude it. Obviously, in the presence of correlations and non-Gaussian errors we cannot simply add the individual log-likelihoods. Instead, we determine the exclusion limits using the log-likelihood q as an estimator.

The first question is how well we can rule out the Standard Model prediction given a data set d_{SUSY} consistent with the superysmmetric Higgs model predictions m_{SUSY}. The purely Standard Model log-likelihood distribution $q(d_{\text{SM}}|m_{\text{SM}})$ usually gives us the desired confidence level as the integral over q from minus infinity to the central value of the m_{SUSY}. However, we also have to take into account that the new-physics data can fluctuate within its experimental and theoretical errors. Basing the statement on one single supersymmetric toy experiment would be incomplete. Therefore, we first compute a 90% confidence level for the Standard Model hypothesis given Standard Model data $\bar{q}$. In a second step we evaluate the log-likelihood distribution for data consistent with the supersymmetric scenario, but still based on the Standard Model couplings $q(d_{\text{SUSY}}|m_{\text{SM}})$.

	Δ_{WWH}	Δ_{ZZH}	Δ_{ttH}	Δ_{bbH}	$\Delta_{\tau\tau H}$	$\Delta_{\gamma\gamma H}$	Δ_{ggH}	m_H
true	-0.01	0.00	0.00	0.14	0.13	0.28	-0.76	112.36
errors	±0.37	±0.53	±0.50	±0.67	±0.62	±0.68	±0.69	±6.83
	-0.41	-1.21	-0.59	-0.39	-0.24	-0.48	-0.59	-1.84
	$+0.32$	$+0.29$	$+0.42$	$+1.10$	$+0.99$	$+0.86$	$+0.79$	$+10.21$

Table 10. Couplings for the gluophobic Higgs scenario. We give the true values of our input and the error bars assuming 10000 toy experiments and 30 fb^{-1} of data.

The percentage of toy experiments giving $q(d_{\text{SUSY}}|m_{\text{SM}}) < \bar{q}$ we find to be 77%. This means that of all our toy experiments assuming the supersymmetric Higgs sector described in table IX, 77% are not described by the Standard Model within the 90% confidence level and can be ruled out accordingly.

The second question is whether the new physics model is a better description of our new physics data (d_{SUSY}) than the Standard Model. The relevant information is the distribution of the difference of the two log-likelihood values for each toy experiment: $\Delta q = q(d_{\text{SUSY}}|m_{\text{SUSY}}) - q(d_{\text{SUSY}}|m_{\text{SM}})$. Note that for most cases we expect this difference to be positive. Because of the non-standard distribution of our log-likelihood the usual definition corresponding to $\Delta\chi^2 > s^2$ (with s a number of standard deviations) does not hold. A detailed discussion on testing different hypotheses and confidence levels we postpone to a later paper, while at this stage we simply request $\Delta q > q_0$ where q_0 is chosen of the order of the quality of the consistently supersymmetric fit. Of all our toy experiments we find that only 4% are better described by the supersymmetric hypothesis than by the Standard Model given this naive choice.

6.2 Gluophobic Higgs

The determination of the Higgs mass plays an important role in the $120 - 140$ GeV mass range because the different branching ratios are steep functions of the mass. For a low-mass Higgs the best mass measurement comes from the decay into two photons, which is usually extracted from overwhelming backgrounds using two side bands. The excellent invariant mass resolution of the detectors then allows for a Higgs mass determination with a dominant experimental error around $\mathcal{O}(100\,\text{MeV})$. However, in models where the loop-induced Higgs couplings to gluons is strongly reduced this mass measurement gets degraded by lower statistics. A supersymmetric Higgs can be a good example for such a possible challenge.

Naively, we would first expect problems with the effective coupling to photons including superpartners. Aside from the usual W and top loop, charged Higgs bosons, sfermions and charginos contribute to the effective coupling of the photons to the Higgs boson. However, the effective $g_{\gamma\gamma H}$ is unlikely to decrease significantly after taking into account current mass limits.

This is different for the inclusive Higgs production rate from gluon fusion. Here, the top loop naturally cancels with the stop loop due to the opposite spin of the two states. Moreover, the current experimental bounds on the stop mass is weak enough to allow for such a scenario, commonly called a gluophobic Higgs. The effect of this supersymmetric scenario on the Higgs parameters we show in the first line of table 10. Similarly to the
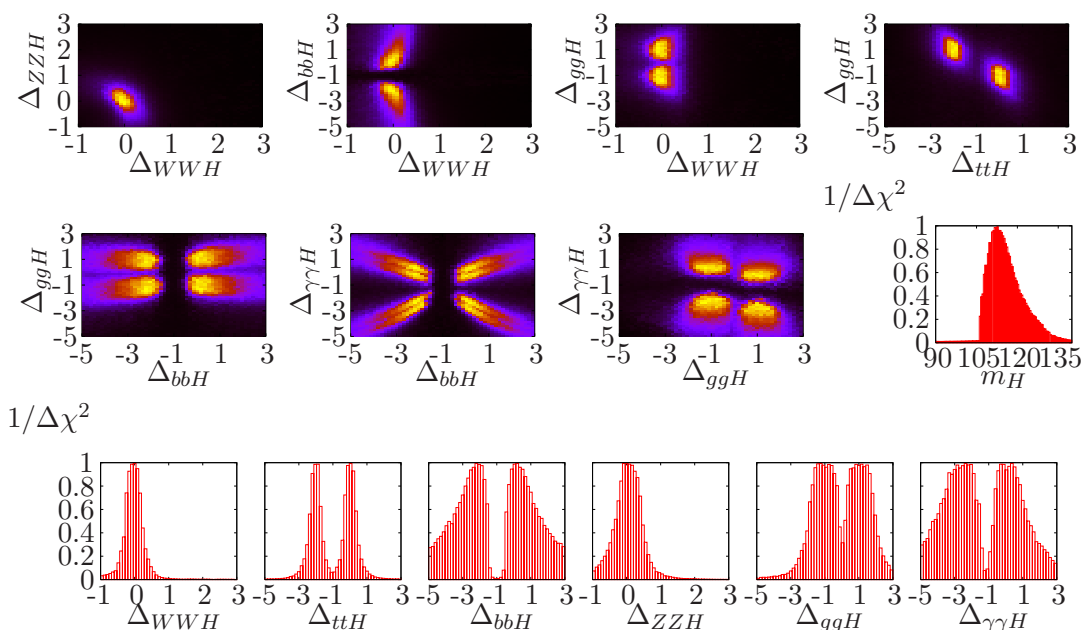
Figure 12. Profile likelihoods for a gluophobic Higgs scenario at 30 fb^{-1}. We include both experimental and theory errors in our analysis.

supersymmetric model shown in table 9 individual deviations from the Standard Model couplings will not be conclusive, and the sizable Δ_{ggH} will turn out to be dangerous, because it reduces the number of Higgs bosons produced altogether and with that the precision on all model parameters.

The reduced rate for the inclusive $H \to \gamma\gamma$ signal means that this channel is no longer suited for a precise determination of the Higgs mass. An alternative is a Higgs decay to ZZ, but for low Higgs masses and strongly reduced inclusive production rates it is even less promising. For an integrated luminosity of 30 fb^{-1} the weak-boson-fusion production process with a subsequent decay to photons predicts 13.5 signal events with a background uncertainty of close to 20 events, which means it will only contribute to a Higgs mass measurement at higher luminosities. The last method for determining the Higgs mass is weak-boson-fusion production with a decay into a τ pair. The $\tau\tau$ invariant mass can be reconstructed in the collinear limit, with a mass resolution around 8 GeV [46, 47], which we assume as the error on the Higgs mass in this scenario.

In figure 12 we show a set of profile likelihoods. The parameter determination suffers from the effective absence of all gluon-fusion production channels and the larger uncertainty in the Higgs boson mass. On the other hand, in contrast to the supersymmetric scenario discussed in section 6.1 we do not observe any severe holes in the analysis. All parameters which do not depend, directly or indirectly, on g_{ggH} are determined well, with an increased error in part from the Higgs mass measurement. This includes g_{WWH}, g_{ZZH}, g_{ttH}, and $g_{\tau\tau H}$. Even for the Δ_{ggH} itself the Standard Model value of zero is excluded. The four solutions for correct and flipped sign of the top-quark coupling and zero or dou-

ble contribution from the additional effective coupling are now grouped in two pairs, each forming a broad peak. This we also observe in the two-dimensional likelihood.

The bbH coupling depends on g_{ggH} via the total width. In the Standard Model loop-induced decays of the Higgs into gluons have a sizable branching ratio. A wide variation in Δ_{ggH} significantly shifts the total width and needs to be compensated by adjusting g_{bbH}, so the decays into bottoms account for the correct rates. The production-side g_{ggH} directly impacts the measurement of $g_{\gamma\gamma H}$. Both, the large range for the gluon coupling and the increased statistical error on the inclusive photon channel lead to a poorer determination of this coupling.

Again, we compute the significance with which we can exclude the Standard Model hypothesis. Follow the prescription outlined in the previous section we find that for 46% of our toy experiments we can rule out the Standard Model at a 90% confidence level. For data consistent with a gluophobic Higgs, the new-physics hypothesis gives a better description than the Standard Model in only 2% of the cases.

7 Outlook

In this paper we have studied quantitatively how well LHC measurements can determine the parameters in the effective weak-scale Higgs sector [11]. SFitter [8] uses Markov chains to map the multi-dimensional Higgs parameter space onto a set of measurements which we expect for a 120 GeV Higgs boson at the LHC. The resulting exclusive likelihood map allows us to show correlations and to determine the error bars for individual Higgs couplings. For an appropriate description of these errors we allow for general correlated statistical, systematic and theory errors. Since we do not find distinct alternative maxima in the exclusive likelihood map, we rely on profile likelihoods (as compared to Bayesian probabilities) to describe likelihood distributions in one or two dimensions.

We find that Higgs couplings can be extracted with typical errors around $20 - 40\%$ using an integrated luminosity of 30 fb^{-1} and properly simulating all errors involved. The different parameters are strongly correlated, and sign ambiguities in particular in the presence of dimension-five operators occur. One main correlation between all channels is due to the total width, which also means that a reliable measurement of the bottom Yukawa coupling for example using subjet analyses [41] is vital for our analysis. Coupling ratios instead of individual couplings can have somewhat reduced errors, also depending on the treatment of the total Higgs width.

Unobservable (not 'invisible') Higgs decays at the LHC can include a coupling to light quarks which also affects the inclusive production cross section. We discuss strategies of dealing with different scenarios of this kind. While the LHC is clearly not going to measure the total Higgs width directly, unexpected effects not contributing to the observed decay channels will be visible in our fit.

Given our results for the error on the couplings it is unlikely that we will be able to use a general Higgs-sector analysis to distinguish between different decoupling model hypotheses (like the MSSM vs Standard Model), but drastic modifications like low-m_A supersymmetry or a gluophobic Higgs boson will be clearly visible. We quantify the confidence levels of

distinguishing the Standard Model hypothesis from the respective new physics hypotheses in a two-dimensional plane, including a possible fluctuation of the data as well as a variation of the model predictions, as predicted by the complete error structure.

Acknowledgments

A   Combining log-likelihoods

For each experimental channel in our analysis we need to combine different sources of errors. The number of events is given by a Poisson distribution which for non-integer event numbers we compute as $P(m,d) = e^{-m}m^d/\Gamma(d+1)$, with m the predicted number of events and d the number of measured events. Systematic errors follow a Gaussian distribution, since they are measured using large background samples. We assume Higgs signals and background measurements of the systematics to be independent. Therefore, their combined probability is the convolution of the individual parts. For two Gaussians this can be done analytically, leading to another Gaussian with the errors added in quadrature. The convolution of a Gaussian and a Poisson distribution, on the other hand, can only be evaluated numerically. This is practically not feasible for each step in our Markov chain, so instead we use an approximate analytic formula.

The basic quantity for SFitter is a generalized χ^2, related to the log-likelihood by $\chi^2 = -2\log L$. First, we transform the Poisson probability into a likelihood L_P. In analogy to the Gaussian case we normalize it to $L(d=m) = 1$. Since the peak of the Poisson distribution is close to $d = m - 0.5$ our likelihood would exceed unity for $d \, \epsilon \, [m-1, m]$. Therefore we fix it to unity in this interval. This way the maximum of a combined Gaussian and Poisson likelihood is well defined and unique at $d = m$. Compared to an exact calculation this method slightly overestimates the likelihood over the whole range, thereby erring on the side of caution. This leads us to

$$-2\log L_P = -2\log\frac{P(m,d)}{P(m,m)} = -2\left[(d-m)\log m + \log\Gamma(m+1) - \log\Gamma(d+1)\right] \quad \text{(A.1)}$$

which in the Gaussian limit becomes $-2\log L_G = (d-m)^2/\sigma^2$ with the combined error σ.
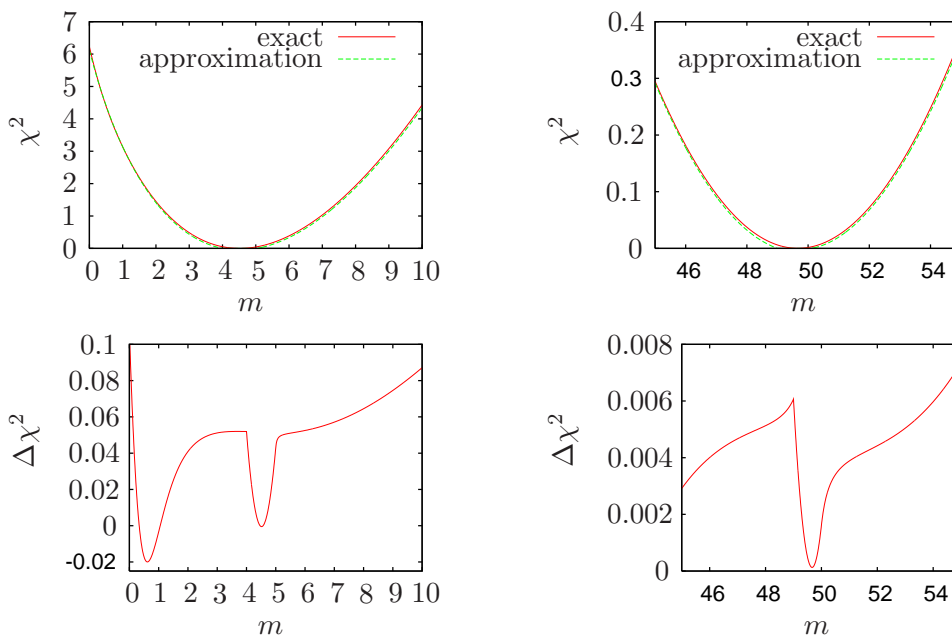
Figure 13. Comparison of our approximate (dashed green) with the exactly convoluted (solid red) log-likelihood. We show the absolute and the relative difference in χ^2 for 5 (left) and 50 (right) events with a Gaussian error of 10%.

Next, we combine the two log-likelihoods into a single form, guided by two limiting cases: the combination of two Gaussians should return the exact formula for the combined Gaussian. Secondly, if one of the log-likelihoods becomes very large, the result should approach the other log-likelihood. The form

$$\frac{1}{\log L} = \frac{1}{\log L_P} + \frac{1}{\log L_G} \qquad \text{or} \qquad \frac{1}{\chi^2} = \frac{-1}{2\log \frac{P(m,d)}{P(m,m)}} + \frac{\sigma_G^2}{(d-m)^2} \qquad (A.2)$$

fulfills both conditions. To test this setup we can compare our result with a numerical convolution for typical cases as they appear in our data. In figure 13 we show results for 5 and 50 events. The Gaussian error is 10%, i.e. 0.5 and 5 respectively. In both cases the difference of our approximation to the exact result is small. Furthermore, we very slightly underestimate χ^2, and consequently slightly overestimate the errors, erring on the safe side.

Note that our results can differ from the naive approach of just multiplying the individual likelihoods arising from different errors for the same channel. This approximation is only valid for different channels in the limit of vanishing correlations between these. We illustrate this for two errors in one channel: let us look at a measurement with two Gaussian distributions with a difference between predicted and measured values x and an error of 1 each. Adding the log-likelihoods gives us $\chi^2 = 2x^2/1^2 = 2x^2$. To compute the standard deviation we set $\chi^2 = 1$ and solve for $x = 1/\sqrt{2}$. In contrast, simply adding both errors in quadrature yields $x = \sqrt{2}$, which means adding the log-likelihoods underestimates the error. This tendency becomes more pronounced when the two errors are not equal.
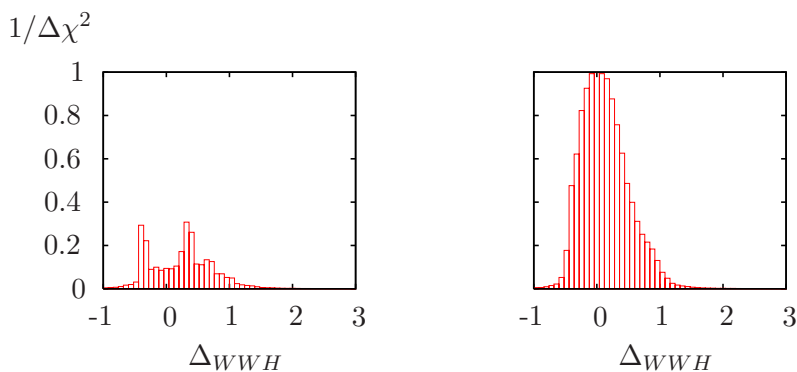
Figure 14. Comparison of profile likelihoods obtained from standard (left) and cooling (right) Markov chains.

B   Cooling Markov chains

The Markov Chain algorithm is optimized for creating Bayesian marginalized log-likelihood distributions. This is analogous to an integration, i.e. not only the height of a peak is relevant for its contribution to the final result, but also its volume in parameter space. Correspondingly, the Metropolis-Hastings algorithm involves two steps: first, it suggests the next point with a probability proportional to the parameter-space volume of a peak structure. Secondly, it accepts or rejects it based on the height of the peak. The total probability is a combination of the two.

In a (frequentist) likelihood approach we are only interested in the height of the peak. Only the value at the tip determines the profile-likelihood value. Following the above argument sharp and high peaks are not very efficiently probed by Markov-Chain algorithms. Consequently, we amend the algorithm so that it better scans the vicinity of points with large function values. A well known approach which does this is simulated annealing [79]. Combining this with the Metropolis-Hastings algorithm [80] we modify the accept or reject condition to

$$\frac{f_{\text{suggested}}}{f_{\text{previous}}} \geq r^{100/(j \cdot c)} \quad , \tag{B.1}$$

where $f_{\text{suggested}}$ and f_{previous} are the function values of the newly suggested and the last point in the Markov chain, respectively. The complete Markov chain we divide into 100 equally long partitions numbered by j. r is a random number between 0 and 1, and c is the cooling factor. We find that $c \sim 10$ gives well-converging results for this analysis. As in the original algorithm a better point is unconditionally accepted.

In the beginning r is almost entirely mapped to values close to $r^{100/c} \sim 0$, i.e. we accept many points and quickly scan the parameter space. As j increases we turn via the standard algorithm into a region where we accept almost only better points. This way we carefully scan the vicinity of the peaks and we obtain reliable values for the profile-likelihood distribution. If there are several peaks of comparable quality, different Markov chains will focus on different peaks. We are guaranteed to see these alternative maxima because we combine 30 individual Markov chains for the final result.

To show the power of this modification we show the one-dimensional profile likelihood for the WWH coupling in figure 14. It includes 30 Markov chains with 200000 points each. We see how the coarse standard algorithm places the peaks at a completely different location while the cooling Markov chain gets both the position and the height of the maximum right (compared to the input).

References

[1] P.W. Higgs, *Broken symmetries, massless particles and gauge fields*, *Phys. Lett.* **12** (1964) 132 [SPIRES];
P.W. Higgs, *Broken symmetries and the masses of gauge bosons*, *Phys. Rev. Lett.* **13** (1964) 508 [SPIRES];
F. Englert and R. Brout, *Broken symmetry and the mass of gauge vector mesons*, *Phys. Rev. Lett.* **13** (1964) 321 [SPIRES].

[2] A. Djouadi, *The Anatomy of electro-weak symmetry breaking. I: The Higgs boson in the standard model*, *Phys. Rept.* **457** (2008) 1 [hep-ph/0503172] [SPIRES];
V. Buescher and K. Jakobs, *Higgs boson searches at hadron colliders*, *Int. J. Mod. Phys.* **A 20** (2005) 2523 [hep-ph/0504099] [SPIRES];
D. Rainwater, *Searching for the Higgs boson*, hep-ph/0702124 [SPIRES].

[3] LEP collaboration, J. Alcaraz et al., *Precision Electroweak Measurements and Constraints on the Standard Model*, arXiv:0712.0929 [SPIRES].

[4] ALEPH collaboration, *Precision Electroweak Measurements and Constraints on the Standard Model*, arXiv:0811.4682 [SPIRES].

[5] See e.g. K.-m. Cheung, *Phenomenology of radion in Randall-Sundrum scenario*, *Phys. Rev.* **D 63** (2001) 056007 [hep-ph/0009232] [SPIRES];
M. Chaichian, A. Datta, K. Huitu and Z.-h. Yu, *Radion and Higgs mixing at the LHC*, *Phys. Lett.* **B 524** (2002) 161 [hep-ph/0110035] [SPIRES];
G.D. Kribs, *Physics of the radion in the Randall-Sundrum scenario*, in Proceedings of *the APS/DPF/DPB Summer Study on the Future of Particle Physics* (Snowmass 2001), ed. N. Graf, Snowmass, Colorado, 30 Jun - 21 Jul 2001, pg. 317 [hep-ph/0110242] [SPIRES];
J.L. Hewett and T.G. Rizzo, *Shifts in the properties of the Higgs boson from radion mixing*, *JHEP* **08** (2003) 028 [hep-ph/0202155] [SPIRES].

[6] For a pedagogical introduction see e.g. S.P. Martin, *A Supersymmetry Primer*, hep-ph/9709356 [SPIRES];
I.J.R. Aitchison, *Supersymmetry and the MSSM: an elementary introduction*, hep-ph/0505105 [SPIRES]; J.F. Gunion and H.E. Haber, *The CP-conserving two-Higgs-doublet model: The approach to the decoupling limit*, *Phys. Rev.* **D 67** (2003) 075019 [hep-ph/0207010] [SPIRES].

[7] H.E. Haber, R. Hempfling and A.H. Hoang, *Approximating the radiatively corrected Higgs mass in the minimal supersymmetric model*, *Z. Phys.* **C 75** (1997) 539 [hep-ph/9609331] [SPIRES];
G. Degrassi, S. Heinemeyer, W. Hollik, P. Slavich and G. Weiglein, *Towards high-precision predictions for the MSSM Higgs sector*, *Eur. Phys. J.* **C 28** (2003) 133 [hep-ph/0212020] [SPIRES];

T. Hahn et al., *Higher-order corrected Higgs bosons in FeynHiggs 2.5*, *Pramana* **69** (2007) 861 [`hep-ph/0611373`] [SPIRES].

[8] R. Lafaye, T. Plehn, M. Rauch and D. Zerwas, *Measuring Supersymmetry*, *Eur. Phys. J.* **C 54** (2008) 617 [`arXiv:0709.3985`] [SPIRES]; for earlier versions of SFitter see: R. Lafaye, T. Plehn and D. Zerwas, *SFITTER: SUSY parameter analysis at LHC and LC*, `hep-ph/0404282` [SPIRES]; R. Lafaye, T. Plehn and D. Zerwas, *SUSY parameter determination*, *ECONF* **C0508141** (2005) ALCPG0607 [`hep-ph/0512028`] [SPIRES].

[9] J.R. Dell'Aquila and C.A. Nelson, *Distinguishing a spin 0 technipion and an elementary Higgs boson: V1 V2 modes with decays into anti-lepton (A) lepton (B) AND/OR anti-q (A) q (B)*, *Phys. Rev.* **D 33** (1986) 93 [SPIRES]; T. Plehn, D.L. Rainwater and D. Zeppenfeld, *Determining the structure of Higgs couplings at the LHC*, *Phys. Rev. Lett.* **88** (2002) 051801 [`hep-ph/0105325`] [SPIRES]; C.P. Buszello, I. Fleck, P. Marquard and J.J. van der Bij, *Prospective analysis of spin- and CP-sensitive variables in $H \to ZZ \to l_1^+ l_1^- l_2^+ l_2^-$ at the LHC*, *Eur. Phys. J.* **C 32** (2004) 209 [`hep-ph/0212396`] [SPIRES]; V. Hankele, G. Klamke, D. Zeppenfeld and T. Figy, *Anomalous Higgs boson couplings in vector boson fusion at the CERN LHC*, *Phys. Rev.* **D 74** (2006) 095001 [`hep-ph/0609075`] [SPIRES]; C. Ruwiedel, N. Wermes and M. Schumacher, *Prospects for the measurement of the structure of the coupling of a Higgs boson to weak gauge bosons in weak boson fusion with the ATLAS detector*, *Eur. Phys. J.* **C 51** (2007) 385 [SPIRES].

[10] D. Zeppenfeld, R. Kinnunen, A. Nikitenko and E. Richter-Was, *Measuring Higgs boson couplings at the LHC*, *Phys. Rev.* **D 62** (2000) 013009 [`hep-ph/0002036`] [SPIRES].

[11] M. Dührssen et al., *Extracting Higgs boson couplings from LHC data*, *Phys. Rev.* **D 70** (2004) 113009 [`hep-ph/0406323`] [SPIRES].

[12] C.P. Burgess, J. Matias and M. Pospelov, *A Higgs or not a Higgs? What to do if you discover a new scalar particle*, *Int. J. Mod. Phys.* **A 17** (2002) 1841 [`hep-ph/9912459`] [SPIRES].

[13] P. Bechtle, K. Desch and P. Wienemann, *Fittino, a program for determining MSSM parameters from collider observables using an iterative method*, *Comput. Phys. Commun.* **174** (2006) 47 [`hep-ph/0412012`] [SPIRES]; P. Bechtle, K. Desch, W. Porod and P. Wienemann, *Determination of MSSM parameters from LHC and ILC observables in a global fit*, *Eur. Phys. J.* **C 46** (2006) 533 [`hep-ph/0511006`] [SPIRES].

[14] T. Plehn and D.L. Rainwater, *Higgs decays to muons in weak boson fusion*, *Phys. Lett.* **B 520** (2001) 108 [`hep-ph/0107180`] [SPIRES]; K. Cranmer and T. Plehn, *Maximum significance at the LHC and Higgs decays to muons*, *Eur. Phys. J.* **C 51** (2007) 415 [`hep-ph/0605268`] [SPIRES]; see also T. Han and B. McElrath, *$H \to \mu^+ \mu^-$ via gluon fusion at the LHC*, *Phys. Lett.* **B 528** (2002) 81 [`hep-ph/0201023`] [SPIRES].

[15] S. Su and B. Thomas, *$H \to mu^+ mu^-$ via tth Production at the LHC*, *Phys. Lett.* **B 677** (2009) 296 [`arXiv:0812.1798`] [SPIRES].

[16] O.J.P. Eboli and D. Zeppenfeld, *Observing an invisible Higgs boson*, *Phys. Lett.* **B 495** (2000) 147 [`hep-ph/0009158`] [SPIRES].

[17] G.C. Cho et al., *Weak boson fusion production of supersymmetric particles at the LHC*, *Phys. Rev.* **D 73** (2006) 054002 [`hep-ph/0601063`] [SPIRES];
J. Alwall, D. Rainwater and T. Plehn, *Same-Sign Charginos and Majorana Neutralinos at the LHC*, *Phys. Rev.* **D 76** (2007) 055006 [`arXiv:0706.0536`] [SPIRES].

[18] U. Baur, T. Plehn and D.L. Rainwater, *Measuring the Higgs boson self coupling at the LHC and finite top mass matrix elements*, *Phys. Rev. Lett.* **89** (2002) 151801 [`hep-ph/0206024`] [SPIRES];
U. Baur, T. Plehn and D.L. Rainwater, *Determining the Higgs boson selfcoupling at hadron colliders*, *Phys. Rev.* **D 67** (2003) 033003 [`hep-ph/0211224`] [SPIRES];
A. Dahlhoff, *Prospects to measure the Higgs boson properties in ATLAS*, `hep-ex/0505022` [SPIRES];
for a different point of view see also F. Gianotti et al., *Physics potential and experimental challenges of the LHC luminosity upgrade*, *Eur. Phys. J.* **C 39** (2005) 293 [`hep-ph/0204087`] [SPIRES].

[19] V. Barger, T. Han, P. Langacker, B. McElrath and P. Zerwas, *Effects of genuine dimension-six Higgs operators*, *Phys. Rev.* **D 67** (2003) 115001 [`hep-ph/0301097`] [SPIRES];
C. Grojean, G. Servant and J.D. Wells, *First-order electroweak phase transition in the standard model with a low cutoff*, *Phys. Rev.* **D 71** (2005) 036001 [`hep-ph/0407019`] [SPIRES];
S. Kanemura, Y. Okada, E. Senaha and C.P. Yuan, *Higgs coupling constants as a probe of new physics*, *Phys. Rev.* **D 70** (2004) 115002 [`hep-ph/0408364`] [SPIRES].

[20] T. Plehn and M. Rauch, *The quartic Higgs coupling at hadron colliders*, *Phys. Rev.* **D 72** (2005) 053008 [`hep-ph/0507321`] [SPIRES];
T. Binoth, S. Karg, N. Kauer and R. Ruckl, *Multi-Higgs boson production in the standard model and beyond*, *Phys. Rev.* **D 74** (2006) 113008 [`hep-ph/0608057`] [SPIRES].

[21] V.D. Barger et al., *CP-violating phases in SUSY, electric dipole moments and linear colliders*, *Phys. Rev.* **D 64** (2001) 056007 [`hep-ph/0101106`] [SPIRES];
S. Abel, S. Khalil and O. Lebedev, *EDM constraints in supersymmetric theories*, *Nucl. Phys.* **B 606** (2001) 151 [`hep-ph/0103320`] [SPIRES];
M. Pospelov and A. Ritz, *Electric dipole moments as probes of new physics*, *Annals Phys.* **318** (2005) 119 [`hep-ph/0504231`] [SPIRES].

[22] M. Spira, A. Djouadi, D. Graudenz and P.M. Zerwas, *Higgs boson production at the LHC*, *Nucl. Phys.* **B 453** (1995) 17 [`hep-ph/9504378`] [SPIRES].

[23] M. Spira, *QCD effects in Higgs physics*, *Fortsch. Phys.* **46** (1998) 203 [`hep-ph/9705337`] [SPIRES].

[24] R.V. Harlander and W.B. Kilgore, *Next-to-next-to-leading order Higgs production at hadron colliders*, *Phys. Rev. Lett.* **88** (2002) 201801 [`hep-ph/0201206`] [SPIRES];
C. Anastasiou and K. Melnikov, *Higgs boson production at hadron colliders in NNLO QCD*, *Nucl. Phys.* **B 646** (2002) 220 [`hep-ph/0207004`] [SPIRES];
V. Ravindran, J. Smith and W.L. van Neerven, *NNLO corrections to the total cross section for Higgs boson production in hadron hadron collisions*, *Nucl. Phys.* **B 665** (2003) 325 [`hep-ph/0302135`] [SPIRES];
C. Anastasiou, R. Boughezal and F. Petriello, *Mixed QCD-electroweak corrections to Higgs boson production in gluon fusion*, *JHEP* **04** (2009) 003 [`arXiv:0811.3458`] [SPIRES].

[25] C. Anastasiou, K. Melnikov and F. Petriello, *The gluon-fusion uncertainty in Higgs coupling extractions*, *Phys. Rev.* **D 72** (2005) 097302 [`hep-ph/0509014`] [SPIRES].

[26] C.A. Nelson, *Correlation between decay planes in Higgs boson decays into W pair (into Z pair)*, *Phys. Rev.* **D 37** (1988) 1220 [SPIRES];
M. Dittmar and H.K. Dreiner, *How to find a Higgs boson with a mass between 155 GeV–180 GeV at the LHC*, *Phys. Rev.* **D 55** (1997) 167 [`hep-ph/9608317`] [SPIRES];
C. Anastasiou, G. Dissertori, F. Stockli and B.R. Webber, *QCD radiation effects on the $H \rightarrow WW \rightarrow l\nu l\nu$ signal at the LHC*, *JHEP* **03** (2008) 017 [`arXiv:0801.2682`] [SPIRES];
M. Grazzini, *NNLO predictions for the Higgs boson signal in the $H \rightarrow WW \rightarrow l\nu l\nu$ and $H \rightarrow ZZ \rightarrow 4l$ decay channels*, *JHEP* **02** (2008) 043 [`arXiv:0801.3232`] [SPIRES].

[27] C. Anastasiou, L.J. Dixon, K. Melnikov and F. Petriello, *High precision QCD at hadron colliders: Electroweak gauge boson rapidity distributions at NNLO*, *Phys. Rev.* **D 69** (2004) 094008 [`hep-ph/0312266`] [SPIRES];
S. Catani and M. Grazzini, *An NNLO subtraction formalism in hadron collisions and its application to Higgs boson production at the LHC*, *Phys. Rev. Lett.* **98** (2007) 222002 [`hep-ph/0703012`] [SPIRES].

[28] S. Catani, D. de Florian, M. Grazzini and P. Nason, *Soft-gluon resummation for Higgs boson production at hadron colliders*, *JHEP* **07** (2003) 028 [`hep-ph/0306211`] [SPIRES];
G. Bozzi, S. Catani, D. de Florian and M. Grazzini, *Transverse-momentum resummation and the spectrum of the Higgs boson at the LHC*, *Nucl. Phys.* **B 737** (2006) 73 [`hep-ph/0508068`] [SPIRES].

[29] V.D. Barger, R.J.N. Phillips and D. Zeppenfeld, *Mini-jet veto: A Tool for the heavy Higgs search at the LHC*, *Phys. Lett.* **B 346** (1995) 106 [`hep-ph/9412276`] [SPIRES];
D.L. Rainwater, R. Szalapski and D. Zeppenfeld, *Probing color singlet exchange in Z + two jet events at the CERN LHC*, *Phys. Rev.* **D 54** (1996) 6680 [`hep-ph/9605444`] [SPIRES];
V. Del Duca et al., *Monte Carlo studies of the jet activity in Higgs + 2jet events*, *JHEP* **10** (2006) 016 [`hep-ph/0608158`] [SPIRES].

[30] T. Han, G. Valencia and S. Willenbrock, *Structure function approach to vector boson scattering in p p collisions*, *Phys. Rev. Lett.* **69** (1992) 3274 [`hep-ph/9206246`] [SPIRES];
T. Figy, C. Oleari and D. Zeppenfeld, *Next-to-leading order jet distributions for Higgs boson production via weak-boson fusion*, *Phys. Rev.* **D 68** (2003) 073005 [`hep-ph/0306109`] [SPIRES];
M. Ciccolini, A. Denner and S. Dittmaier, *Strong and electroweak corrections to the production of Higgs+2jets via weak interactions at the LHC*, *Phys. Rev. Lett.* **99** (2007) 161803 [`arXiv:0707.0381`] [SPIRES];
M. Ciccolini, A. Denner and S. Dittmaier, *Electroweak and QCD corrections to Higgs production via vector-boson fusion at the LHC*, *Phys. Rev.* **D 77** (2008) 013002 [`arXiv:0710.4749`] [SPIRES];
K. Arnold et al., *VBFNLO: A parton level Monte Carlo for processes with electroweak bosons*, `arXiv:0811.4559` [SPIRES].

[31] J.R. Andersen, T. Binoth, G. Heinrich and J.M. Smillie, *Loop induced interference effects in Higgs Boson plus two jet production at the LHC*, *JHEP* **02** (2008) 057 [`arXiv:0709.3513`] [SPIRES];
A. Bredenstein, K. Hagiwara and B. Jager, *Mixed QCD-electroweak contributions to Higgs-plus-dijet production at the LHC*, *Phys. Rev.* **D 77** (2008) 073004 [`arXiv:0801.4231`] [SPIRES].

[32] K. Cranmer et al., *Prospects for Higgs searches via VBF at the LHC with the ATLAS detector*, `hep-ph/0401148` [SPIRES].

[33] J.R. Forshaw and M. Sjodahl, *Soft gluons in Higgs plus two jet production*, *JHEP* **09** (2007) 119 [`arXiv:0705.1504`] [SPIRES];
J.R. Andersen, V. Del Duca and C.D. White, *Higgs Boson Production in Association with Multiple Hard Jets*, *JHEP* **02** (2009) 015 [`arXiv:0808.3696`] [SPIRES].

[34] V. Del Duca, W. Kilgore, C. Oleari, C. Schmidt and D. Zeppenfeld, *H + 2 jets via gluon fusion*, *Phys. Rev. Lett.* **87** (2001) 122001 [`hep-ph/0105129`] [SPIRES];
A. Nikitenko and M. Vazquez Acosta, *Monte Carlo study of $gg \to H + jets$ contribution to Vector Boson Fusion Higgs production at the LHC*, `arXiv:0705.3585` [SPIRES].

[35] W. Beenakker et al., *Higgs radiation off top quarks at the Tevatron and the LHC*, *Phys. Rev. Lett.* **87** (2001) 201805 [`hep-ph/0107081`] [SPIRES]; *NLO QCD corrections to t anti-t H production in hadron collisions*, *Nucl. Phys.* **B 653** (2003) 151 [`hep-ph/0211352`] [SPIRES];
S. Dawson, L.H. Orr, L. Reina and D. Wackeroth, *Associated top quark Higgs boson production at the LHC*, *Phys. Rev.* **D 67** (2003) 071503 [`hep-ph/0211438`] [SPIRES].

[36] D.A. Dicus, C. Kao and S.S.D. Willenbrock, *Higgs boson pair production from gluon fusion*, *Phys. Lett.* **B 203** (1988) 457 [SPIRES];
E.W.N. Glover and J.J. van der Bij, *Higgs boson pair production via gluon fusion*, *Nucl. Phys.* **B 309** (1988) 282 [SPIRES];
T. Plehn, M. Spira and P.M. Zerwas, *Pair Production of Neutral Higgs Particles in Gluon-Gluon Collisions*, *Nucl. Phys.* **B 479** (1996) 46 [*Erratum ibid.* **B 531** (1998) 655] [`hep-ph/9603205`] [SPIRES];
A. Djouadi, W. Kilian, M. Muhlleitner and P.M. Zerwas, *Production of neutral Higgs-boson pairs at LHC*, *Eur. Phys. J.* **C 10** (1999) 45 [`hep-ph/9904287`] [SPIRES];
S. Dawson, S. Dittmaier and M. Spira, *Neutral Higgs-boson pair production at hadron colliders: QCD corrections*, *Phys. Rev.* **D 58** (1998) 115012 [`hep-ph/9805244`] [SPIRES].

[37] U. Baur, T. Plehn and D.L. Rainwater, *Probing the Higgs selfcoupling at hadron colliders using rare decays*, *Phys. Rev.* **D 69** (2004) 053004 [`hep-ph/0310056`] [SPIRES].

[38] See also S. Asai et al., *Prospects for the search for a standard model Higgs boson in ATLAS using vector boson fusion*, *Eur. Phys. J.* **C32S2** (2004) 19 [`hep-ph/0402254`] [SPIRES];
S. Abdullin et al., *Summary of the CMS potential for the Higgs boson discovery*, *Eur. Phys. J.* **C39S2** (2005) 41.

[39] E. Richter-Was and M. Sapinski, *Search for the SM and MSSM Higgs boson in the $t\bar{t}H, H \to b\bar{b}$ channel*, *Acta Phys. Polon.* **B 30** (1999) 1001 [SPIRES];
V. Drollinger, T. Müller and D. Denegri, *Searching for Higgs bosons in association with top quark pairs in the $H0 \to b$ anti-b decay mode*, `hep-ph/0111312` [SPIRES];
V. Kostioukhine, J. Leveque, A. Rozanov and J.B. de Vivie, *Search for the standard model Higgs Boson in the ttH, $H \to WW$ channel*, ATL-PHYS-2002-019;
J. Cammin and M. Schumacher, *The ATLAS discovery potential for the channel ttH, $H \to bb$*, ATL-PHYS-2003-024.

[40] V. Drollinger, T. Müller and D. Denegri, *Prospects for Higgs boson searches in the channel $W^{\pm}H^0 \to l^{\pm}\nu b\bar{b}$*, `hep-ph/0201249` [SPIRES];
J.M. Campbell, R.K. Ellis and D.L. Rainwater, *Next-to-leading order QCD predictions for W + 2jet and Z + 2jet production at the CERN LHC*, *Phys. Rev.* **D 68** (2003) 094021 [`hep-ph/0308195`] [SPIRES].

[41] J.M. Butterworth, A.R. Davison, M. Rubin and G.P. Salam, *Jet substructure as a new Higgs search channel at the LHC*, *Phys. Rev. Lett.* **100** (2008) 242001 [`arXiv:0802.2470`] [SPIRES].

[42] D.L. Rainwater and D. Zeppenfeld, *Observing $H \to W^{(*)}W^{(*)} \to e^{\pm}\mu^{\mp}\not{p}_T$ in weak boson fusion with dual forward jet tagging at the CERN LHC*, *Phys. Rev.* **D 60** (1999) 113004 [*Erratum ibid.* **D 61** (2000) 099901] [`hep-ph/9906218`] [SPIRES];
N. Kauer, T. Plehn, D.L. Rainwater and D. Zeppenfeld, *H → W W as the discovery mode for a light Higgs boson*, *Phys. Lett.* **B 503** (2001) 113 [`hep-ph/0012351`] [SPIRES];
N. Akchurin et al., *120-180 gev Higgs in $qq \to qqh$ Channel at CMS*, CMS-NOTE-2002-066;
B. Mellado, *Prospects of Higgs Physics at the LHC*, ATL-CONF-2002-004 [`hep-ex/0211062`];
S. Asai et al., *Prospects for the Search of a Standard Model Higgs Boson in ATLAS using Vector Boson Fusion*, *Eur. Phys. J* **C 32** (2004) s19 [ATL-PHYS-2003-005];
G. Azuelos and R. Mazini, *Searching for $H \to \nu^{+}\nu^{-} \to l\nu_l\nu_\tau$ by Vector Boson Fusion in ATLAS*, ATL-PHYS-2003-004.

[43] F. Maltoni, D.L. Rainwater and S. Willenbrock, *Measuring the top-quark Yukawa coupling at hadron colliders via $t\bar{t}h, h \to W^{+}W^{-}$*, *Phys. Rev.* **D 66** (2002) 034022 [`hep-ph/0202205`] [SPIRES].

[44] K. Cranmer, B. Mellado, W. Quayle and S.L. Wu, *Application of K factors in the $H \to ZZ^{*} \to 4l$ analysis at the LHC*, `hep-ph/0307242` [SPIRES].

[45] E. Yazgan et al., *Search for a standard model Higgs boson in CMS via vector boson fusion in the $H \to WW \to \ell\nu\ell\nu$ channel*, *Eur. Phys. J.* **C 53** (2008) 329 [`arXiv:0706.1898`] [SPIRES].

[46] R.K. Ellis, I. Hinchliffe, M. Soldate and J.J. van der Bij, *Higgs Decay to tau+ tau-: A Possible Signature of Intermediate Mass Higgs Bosons at the SSC*, *Nucl. Phys.* **B 297** (1988) 221 [SPIRES].

[47] D.L. Rainwater, D. Zeppenfeld and K. Hagiwara, *Searching for $H \to \tau\tau$ in weak boson fusion at the LHC*, *Phys. Rev.* **D 59** (1999) 014037 [`hep-ph/9808468`] [SPIRES];
T. Plehn, D.L. Rainwater and D. Zeppenfeld, *A method for identifying $H \to \tau\tau \to e^{\pm}\mu^{\mp}$ missing p_T at the CERN LHC*, *Phys. Rev.* **D 61** (2000) 093005 [`hep-ph/9911385`] [SPIRES].

[48] K. Cranmer, B. Mellado, W. Quayle and S.L. Wu, *An update of the VBF Htautau cut analysis*, ATLAS internal note ATL-COM-PHYS-2003-002 (2003).

[49] A. Belyaev and L. Reina, *$pp \to ttH, H \to \tau\tau$: toward a model independent determination of the Higgs boson couplings at the LHC*, *JHEP* **08** (2002) 041 [`hep-ph/0205270`] [SPIRES].

[50] S. Abdullin et al., *Higgs boson discovery potential of LHC in the channel $pp \to \gamma\gamma + jet$*, *Phys. Lett.* **B 431** (1998) 410 [`hep-ph/9805341`] [SPIRES];
F. Stockli, A.G. Holzner and G. Dissertori, *Study of perturbative QCD predictions at next-to-leading order and beyond for $p\,p \to H \to \gamma\gamma + X$*, *JHEP* **10** (2005) 079 [`hep-ph/0509130`] [SPIRES].

[51] D.L. Rainwater and D. Zeppenfeld, *Searching for $H \to \gamma\gamma$ in weak boson fusion at the LHC*, *JHEP* **12** (1997) 005 [`hep-ph/9712271`] [SPIRES];
K. Cranmer, B. Mellado, W. Quayle and S.L. Wu, *Search for Higgs bosons decay $H \to \gamma\gamma$ using vector boson fusion*, `hep-ph/0401088` [SPIRES].

[52] G. Eynard, *Study of associated Higgs boson production $HW, Ht\bar{t}, HZ \to \gamma\gamma + e^{\pm}/\mu^{\pm} + X$ with the ATLAS detector at LHC* (in French), CERN-THESIS-2000-036 (1998).

[53] R.M. Godbole, M. Guchait, K. Mazumdar, S. Moretti and D.P. Roy, *Search for 'invisible' Higgs signals at LHC via associated production with gauge bosons*, *Phys. Lett.* **B 571** (2003) 184 [`hep-ph/0304137`] [SPIRES].

[54] M.L. Mangano, M. Moretti, F. Piccinini, R. Pittau and A.D. Polosa, *$b\bar{b}$ final states in Higgs production via weak boson fusion at the LHC*, *Phys. Lett.* **B 556** (2003) 50 [`hep-ph/0210261`] [SPIRES].

[55] D.L. Rainwater, *A new method for measuring the bottom quark Yukawa coupling at the CERN Large Hadron Collider*, *Phys. Lett.* **B 503** (2001) 320 [`hep-ph/0004119`] [SPIRES].

[56] A. Ballestrero, G. Bevilacqua and E. Maina, *A new analysis of $PP \to bbl\nu jj$ at the LHC: Higgs and W boson associated production with two tag jets*, *JHEP* **08** (2008) 059 [`arXiv:0806.4075`] [SPIRES].

[57] E. Gabrielli et al., *Higgs boson production in association with a photon in vector boson fusion at the LHC*, *Nucl. Phys.* **B 781** (2007) 64 [`hep-ph/0702119`] [SPIRES].

[58] M. Spira, *HIGLU: A Program for the Calculation of the Total Higgs Production Cross Section at Hadron Colliders via Gluon Fusion including QCD Corrections*, `hep-ph/9510347` [SPIRES].

[59] A. Djouadi, J. Kalinowski and M. Spira, *HDECAY: A program for Higgs boson decays in the standard model and its supersymmetric extension*, *Comput. Phys. Commun.* **108** (1998) 56 [`hep-ph/9704448`] [SPIRES].

[60] M. Dührssen, *Prospects for the measurement of Higgs boson coupling parameters in the mass range from 110–190 GeV/c2*, ATL-PHYS-2003-030.

[61] THE ATLAS collaboration, G. Aad et al., *Expected Performance of the ATLAS Experiment-Detector, Trigger and Physics*, `arXiv:0901.0512` [SPIRES].

[62] CMS collaboration, G.L. Bayatian et al., *CMS technical design report, volume II: Physics performance*, *J. Phys.* **G 34** (2007) 995 [SPIRES].

[63] A. Hocker, H. Lacker, S. Laplace and F. Le Diberder, *A New approach to a global fit of the CKM matrix*, *Eur. Phys. J.* **C 21** (2001) 225 [`hep-ph/0104062`] [SPIRES];
J. Charles, A. Hocker, H. Lacker, F.R. Le Diberder and S. T'Jampens, *Bayesian statistics at work: the troublesome extraction of the CKM phase alpha*, `hep-ph/0607246` [SPIRES].

[64] See e.g. G.D. Kribs, T. Plehn, M. Spannowsky and T.M.P. Tait, *Four generations and Higgs physics*, *Phys. Rev.* **D 76** (2007) 075016 [`arXiv:0706.3718`] [SPIRES].

[65] C. Arnesen, I.Z. Rothstein and J. Zupan, *Smoking Guns for On-Shell New Physics at the LHC*, `arXiv:0809.1429` [SPIRES].

[66] For a survey of new-physics effects see e.g. G. Cacciapaglia, A. Deandrea and J. Llodra-Perez, *Higgs to Gamma Gamma beyond the Standard Model*, *JHEP* **06** (2009) 054 [`arXiv:0901.0927`] [SPIRES].

[67] E.A. Baltz and P. Gondolo, *Markov chain Monte Carlo exploration of minimal supergravity with implications for dark matter*, *JHEP* **10** (2004) 052 [`hep-ph/0407039`] [SPIRES];
E.A. Baltz, M. Battaglia, M.E. Peskin and T. Wizansky, *Determination of dark matter properties at high-energy colliders*, *Phys. Rev.* **D 74** (2006) 103521 [`hep-ph/0602187`] [SPIRES].

[68] B.C. Allanach and C.G. Lester, *Multi-Dimensional mSUGRA Likelihood Maps*, *Phys. Rev.* **D 73** (2006) 015013 [`hep-ph/0507283`] [SPIRES];
B.C. Allanach, *Naturalness priors and fits to the constrained minimal supersymmetric standard model*, *Phys. Lett.* **B 635** (2006) 123 [`hep-ph/0601089`] [SPIRES];
B.C. Allanach, K. Cranmer, C.G. Lester and A.M. Weber, *Natural Priors, CMSSM Fits and LHC Weather Forecasts*, *JHEP* **08** (2007) 023 [`arXiv:0705.0487`] [SPIRES].

[69] R.R. de Austri, R. Trotta and L. Roszkowski, *A Markov chain Monte Carlo analysis of the CMSSM*, *JHEP* **05** (2006) 002 [`hep-ph/0602028`] [SPIRES];
R. Trotta, R. Ruiz de Austri and L. Roszkowski, *Direct dark matter detection around the corner? Prospects in the constrained MSSM*, *J. Phys. Conf. Ser.* **60** (2007) 259 [SPIRES];
Prospects for direct dark matter detection in the constrained MSSM, *New Astron. Rev.* **51** (2007) 316 [`astro-ph/0609126`] [SPIRES];
L. Roszkowski, R.R. de Austri, J. Silk and R. Trotta, *On prospects for dark matter indirect detection in the Constrained MSSM*, *Phys. Lett.* **B 671** (2009) 10 [`arXiv:0707.0622`] [SPIRES].

[70] TEVATRON ELECTROWEAK WORKING GROUP collaboration, *Combination of CDF and D0 Results on the Mass of the Top Quark*, `arXiv:0903.2503` [SPIRES].

[71] See e.g. U. Ellwanger, J.F. Gunion and C. Hugonie, *Difficult scenarios for NMSSM Higgs discovery at the LHC*, *JHEP* **07** (2005) 041 [`hep-ph/0503203`] [SPIRES];
A. Martin, *Higgs cascade decays to gamma gamma + jet jet at the LHC*, `hep-ph/0703247` [SPIRES];
M. Carena, T. Han, G.Y. Huang and C.E.M. Wagner, *Higgs Signal for $h \to aa$ at Hadron Colliders*, *JHEP* **04** (2008) 092 [`arXiv:0712.2466`] [SPIRES];
S. Chang, R. Dermisek, J.F. Gunion and N. Weiner, *Nonstandard Higgs Boson Decays*, *Ann. Rev. Nucl. Part. Sci.* **58** (2008) 75 [`arXiv:0801.4554`] [SPIRES];
S. Chang and T. Gregoire, *Discovering a Nonstandard Higgs in a Standard Way*, `arXiv:0903.0403` [SPIRES].

[72] A. Alves, O. Éboli, T. Plehn and D.L. Rainwater, *Robust LHC Higgs search in weak boson fusion*, *Phys. Rev.* **D 69** (2004) 075005 [`hep-ph/0309042`] [SPIRES].

[73] T. Plehn, D.L. Rainwater and D. Zeppenfeld, *Probing the MSSM Higgs sector via weak boson fusion at the LHC*, *Phys. Lett.* **B 454** (1999) 297 [`hep-ph/9902434`] [SPIRES];
T. Plehn, D.L. Rainwater and D. Zeppenfeld, *A method for identifying $H \to \tau\tau \to e^{\pm}\mu^{\mp}$ missing p_T at the CERN LHC*, *Phys. Rev.* **D 61** (2000) 093005 [`hep-ph/9911385`] [SPIRES];
M. Schumacher, *Investigation of the discovery potential for Higgs bosons of the minimal supersymmetric extension of the standard model (MSSM) with ATLAS*, `hep-ph/0410112` [SPIRES].

[74] A. Djouadi, *Squark effects on Higgs boson production and decay at the LHC*, *Phys. Lett.* **B 435** (1998) 101 [`hep-ph/9806315`] [SPIRES].

[75] B.C. Allanach et al., *The Snowmass points and slopes: Benchmarks for SUSY searches*, *Eur. Phys. J.* **C 25** (2002) 113 [*eConf* **C010630** (2001) P125] [`hep-ph/0202233`] [SPIRES].

[76] A. Djouadi, J.-L. Kneur and G. Moultaka, *SuSpect: A Fortran code for the supersymmetric and Higgs particle spectrum in the MSSM*, *Comput. Phys. Commun.* **176** (2007) 426 [`hep-ph/0211331`] [SPIRES].

[77] W. Hollik, T. Plehn, M. Rauch and H. Rzehak, *Supersymmetric Higgs Bosons in Weak Boson Fusion*, *Phys. Rev. Lett.* **102** (2009) 091802 [`arXiv:0804.2676`] [SPIRES].

[78] R.V. Harlander and M. Steinhauser, *Hadronic Higgs production and decay in supersymmetry at next-to-leading order*, *Phys. Lett.* **B 574** (2003) 258 [`hep-ph/0307346`] [SPIRES];
R.V. Harlander and M. Steinhauser, *Supersymmetric Higgs production in gluon fusion at next-to-leading order*, *JHEP* **09** (2004) 066 [`hep-ph/0409010`] [SPIRES];
C. Anastasiou, S. Beerli and A. Daleo, *The two-loop QCD amplitude $gg \to h, H$ in the Minimal Supersymmetric Standard Model*, *Phys. Rev. Lett.* **100** (2008) 241806 [`arXiv:0803.3065`] [SPIRES].

[79] S. Kirkpatrick, C.D. Gelatt and M.P. Vecchi, *Optimization by Simulated Annealing*, *Science* **220** (1983) 671;
A. Corana, M. Marchesi, C. Martini and S. Ridella, *Minimizing multimodal functions of continuous variables with the "simulated annealing" algorithm*, *ACM Trans. Math. Softw.* **13** (1987) 3.

[80] N. Metropolis, A.W. Rosenbluth, M.N. Teller and E. Teller, *Equations of State Calculations by Fast Computing Machines*, *J. Chem. Phys.* **21** (1953) 1087;
W.K. Hastings, *Monte Carlo Sampling Methods Using Markov Chains and Their Applications*, *Biometrika* **57** (1970) 97.